# LIBRARY Michigan State University

PLACE IN RETURN BOX to remove this checkout from your record. TO AVOID FINES return on or before date due.

| DATE DUE | DATE DUE | DATE DUE |
|----------|----------|----------|
| [1][412] |          |          |
| 221      |          |          |
|          |          |          |
|          |          |          |
|          |          |          |
|          |          |          |
|          |          |          |

MSU Is An Affirmative Action/Equal Opportunity Institution

c:\circ\datedue.pm3-p.1

## TEXTURE AND BIMODAL GRAIN GROWTH IN B2 FeAl ALLOYS

Ву

James Stout

### A THESIS

Submitted to
Michigan State University
for partial fulfillment of the requirements
for the degree of

## MASTERS OF SCIENCE

Department of Material Science and Mechanics
1992

Abnormal heat treated containing develops during to produce to and run partisalso developed been developed stringers at grain grown cast billed cleaner mobserved.

developed

the identi

#### **ABSTRACT**

#### TEXTURE AND BIMODAL GRAIN GROWTH IN B2 FeAl ALLOYS

By

#### James Stout

Abnormal grain growth has been observed in B2 FeAl alloys heat treated above 1000°C. An equiaxed micro-structure containing a relatively high volume of oxide stringers develops during the powder processing technique commonly used to produce these alloys. The oxide stringers are well aligned and run parallel to the extrusion axis. A <111> wire texture is also developed during the powder processing. A theory has been developed proposing that the combination of the oxide stringers and the wire texture is responsible for the abnormal grain growth. Similar materials produced by hot extrusion of cast billets were also examined. These materials had much cleaner microstructures and no abnormal grain growth was observed. The effect extrusion temperature has on texture was also examined. It was found that material extruded at 1077°C developed a significantly stronger <111> wire texture then did the identical material extruded at 800°C.

I would for their and friend appreciate Dr. Tom B this study support of Program.

Center to NAG 3-56
National

parents,

been pos

#### **ACKNOWLEDGEMENTS**

I would like to express my thanks to a number of people for their assistance in completing this work. The guidance and friendship of my advisor Dr. Martin A. Crimp was greatly appreciated and acknowledged. I would also like to thank Dr. Tom Bieler for the informative discussions we had during this study. I would like to acknowledge the financial support of Michigan State University through the AURIG Program. Materials were obtained from NASA Lewis Research Center through Case Western Reserve University under grant NAG 3-563. The popLA software was obtained from Los Alamos National Laboratory. And finally, I'd like to thank my parents, the safety net, without whom this would not have been possible.

I. INTRO

II. PRO

III. RE

IA. Di

# TABLE OF CONTENTS

|      |  | page     |
|------|--|----------|
| I.   | INTRODUCTION                             | 1        |
|      | Grain Growth                             | 4        |
|      | Grain Boundaries                         | 5<br>8   |
|      | The Coincidence Site Lattice Boundary    |          |
|      | The Dislocation Boundary                 | 14       |
|      | Summary (Grain Boundaries)               | 18       |
|      | Grain Boundary Energy and Mobility       | 18       |
|      | Grain Boundary Migration                 | 18       |
|      | Dislocation Migration                    | 18       |
|      | Vapor Mechanisms                         | 19       |
|      | Diffusion Mechanisms                     | 20       |
|      | Orientation Dependence of Migration Rate | 22       |
|      | Summary (Grain Boundary Migration)       | 26       |
|      | Grain Growth                             | 27       |
|      | Recrystallization                        | 29       |
|      | Texture and Grain Growth in FeAl         | 32       |
| II.  | PROCEDURE                                | 34       |
|      | Materials                                | 34       |
|      | Sample Preparation                       | 36       |
|      | X-Ray Analysis                           | 36<br>39 |
| ***  | EBSP Analysis RESULTS                    | 44       |
| 111. |  | 44       |
|      | Optical Microscopy                       | 52       |
|      | X-Ray Analysis Powder Processed Material | 52<br>53 |
|      | Cast Material                            | 78       |
|      | EBSP Results                             | 81       |
| IV.  | DISCUSSION                               | 93       |
| 1.   | Powder Processed Material                | 94       |
|      | The As-Extruded State                    | 94       |
|      | Microstructure                           | 94       |
|      | Extrusion Temperature and Grain Size     | 96       |
|      | Composition                              | 97       |
|      | Texture                                  | 97       |
|      | The Effect of Temperature on Texture     | 99       |
|      | After 1000°C Heat Treatment              | 100      |
|      | Microstructure                           | 100      |
|      | Texture                                  | 101      |
|      | After 1050/1100°C Heat Treatment         | 101      |
|      | Microstructure                           | 101      |
|      | Microstructure and Texture               | 102      |
|      | A Theory on Bimodal Grain Growth in Wire |          |
|      | Textured Materials                       | 109      |
|      | Texture                                  | 112      |
|      | Macroscopic Behavior                     | 114      |
|      | After 1200°C Heat Treatment              | 116      |
|      | Microstructure                           | 116      |
|      | Texture                                  | 116      |
|      | Cast Material                            | 117      |
|      | Microstructure                           | 117      |
|      | Texture                                  | 118      |

Conne

V. CONCLUS

VI. REFEREN

VII. APPENDI

|      | Comments                      | 119 |
|------|-------------------------------|-----|
| v.   | CONCLUSIONS                   | 121 |
| VI.  | REFERENCES                    | 123 |
| VII. | APPENDIX A - extrusion sheets | 128 |

fable I.

fable II. Che

Ang CSL

Table III. Gra

Table IV.

Com; beta the

## LIST OF TABLES

|       |      | n  | aqe |
|-------|------|--|-----|
| Table | I.   | Angles of misorientation for various common CSL situations [48].                                       | 9   |
| Table | II.  | Chemical analysis of FeAl alloys after extrusion [3].  | 35  |
| Table | III. | Grain sizes of the FeAl alloys before and after heat treatments [3].                                   | 45  |
| Table | IV.  | Comparison of relative peak intensities between FeAl powder from published data and the extruded form. | 52  |

Figure 1.

Figure 2.

Figure 3.

Figure 4.

Figure 5.

Pigure 6

Pigure 7

Pigure 8

Pigure 9

Pigure :

Pigure :

Pigure

# LIST OF FIGURES

| Figure | 1.  | The unit cell of B2 FeAl alloys.   | page<br>2 |
|--------|-----|--|-----------|
| Figure | 2.  | Diagram of low angle symmetric tilt<br>boundaries. (a) How crystals may appear if<br>separated. (b) Dislocation structure after<br>joining. [36]   | 6         |
| Figure | 3.  | Two crystals rotated 38° to form a CSL relationship. The black dots represent the coincidence lattice common to both crystals [37].  | 9         |
| Figure | 4.  | Periodic adjustments at grain boundaries as described by Bishop and Chalmers [25].   | 12        |
| Figure | 5.  | (a) 37° <001> tilt boundary. The lattices are placed so that the lattice sites are shared in the boundary. (b) The same 37° <001> tilt boundary with the two crystals displaced so no lattice positions are shared [26]. | 13        |
| Figure | 6.  | (a) Dislocation model of a 53° symmetric tilt boundary. (b) Dislocation model of a 60° symmetric tilt boundary [37].   | 15        |
| Figure | 7.  | <ul><li>(a) A boundary having no coalescence,</li><li>(b) partial coalescence, and (c) total coalescence [30].</li></ul>   | 17        |
| Figure | 8.  | Partially coalesced boundary with an array of dislocations screening the boundary from the matrix [30].  | 17        |
| Figure | 9.  | The free energy diagram of an atom crossing a narrow grain boundary [35].  | 22        |
| Figure | 10  | Rate of boundary migration at 300°C as a function of tin concentration in zone refined lead, for random and special angle boundaries [18].   | 24        |
| Figure | 11. | Activation energy for boundary migration as a function of tin concentration in zone refined lead for random and special angle boundaries [18].   | 24        |
| Figure | 12. | . Diffraction pattern of FeAl alloy produced from powder processing using Cu kα radiation  | 38        |

Pigure 13. Ill Pigure 14. EBS us: fil Figure 15. Mic 40a (a) (b) Figure 16. Mid 40 tr lo Figure 17. Mi 40 24 Figure 18. Mi Figure 19. Po Figure 20. I

e) Lo

p: { a

Figure 21. J

Pigure 22.

| Figure | 13. | Illustration of the set up used to produce EBSP images.  | 40 |
|--------|-----|--|----|
| Figure | 14. | EBSP image generated from a FeAl sample using a 20kV accelerating voltage on a LaB <sub>6</sub> filament.  | 43 |
| Figure | 15. | Micrographs of powder processed Fe-<br>40at%Al+0.1B single extruded 16:1 showing<br>(a) the longitudinal view [3] and<br>(b) the transverse [3].   | 46 |
| Figure | 16. | Micrographs of powder processed Fe-40at%Al+0.1B single extruded 16:1 and heat treated 24 hrs. at 1100°C, (a) shows the longitudinal view [3] and (b) the transverse.   | 48 |
| Figure | 17. | Micrograph of powder processed Fe-<br>40at%Al+0.1B extruded 16:1 and heat treated<br>24 hrs. at 1200°C, Transverse view.   | 49 |
| Figure | 18. | Micrograph of cast Fe-40at%Al+0.1B extruded 16:1 in the as extruded state [3]. Longitudinal view.  | 51 |
| Figure | 19. | Pole figures generated from a powder processed FeAl alloy, (a) displays the {111} family of planes, (b) the {110} and (c) the {211}.   | 54 |
| Figure | 20. | Inverse pole figures for the powder processed Fe-40at%Al material extruded 16:1, (a) displays the texture prior to heat treatment, (b) the 1000°C, (c) the 1100°C none grain growth, (d) the 1100°C with bimodal grain growth.   | 58 |
| Figure | 21. | Inverse pole figures for the powder processed Fe-40at%Al+0.1B material extruded 16:1, (a) displays the texture prior to heat treatment, (b) after 1000°C, (c) after 1100°C with no little grain growth, (d) after 1100°C with bimodal grain growth and (e) after 1200°C. | 64 |
| Figure | 22. | Inverse pole figures of the powder processed Fe-40at%Al+0.2B material double extruded, (a) displays the texture prior to heat treatment, (b) after 1000°C and  | 69 |

| Figure | 23. | Inverse pole figures of powder processed Fe-40at*Al single and double extruded, (a) single extruded 8:1 at 977°C, (b) after a second 6:1 extrusion at 800°C and (c) after a second 6:1 extrusion at 1077°C.   | 73                |
|--------|-----|---|-------------------|
| Figure | 24. | Inverse pole figures of double extruded Fe-50at%Al receiving the second extrusion at different temperatures, (a) second extrusion at 800°C and (b) at 1077°C.   | 76                |
| Figure | 25. | Inverse pole figure of the Fe-40at%Al cast and extruded material.   | 79                |
| Figure | 26. | Inverse pole figure of Fe-40at%Al+0.1B cast and extruded material.  | 80                |
| Figure | 27. | Inverse texture plots for the 16:1 single extruded Fe-40at%Al material, (a) shows orientations from grains prior to heat treatment, (b) after 1000°C, (c) after 1100°C with little grain growth and (d) after 1100°C with bimodal grain growth.                         | 83                |
| Figure | 1   | Inverse texture plots of the 16:1 single extruded Fe-40at*Al+0.1B material, (a) shows orientations from grains prior to heat treatment, (b) after 1000°C, (c) after 1100°C from original matrix grains, (d) after 1100°C from abnormal grains only and (e) after 1200°C | 87                |
| Figure | 29. | Inverse texture plot for the double extruded Fe-40at*Al+0.2B material, (a) shows orientation from grains after 1050°C heat treatment from original matrix grains only and (b) after 1050°C heat treatment from abnormal grains only.                                    | 91                |
| Figure | 30. | Inverse texture plot of cast and extruded Fe-40at%Al+0.1B.  | 92                |
| Figure | 31. | Illustration of rotational freedom in a material with a wire texture. After Hazzledine [74].  | 104               |
| Figure | 32. | The two geometries of a grain boundary/ particle interaction as discussed above [65].   | 108               |
| Figure | 33. | Plots of the relative drag forces produced<br>by an ellipsoidal particle for variations<br>in eccentricity for the two cases described<br>above. The forces are normalized against the<br>drag force of a spherical particle F, [65].                                   | 108<br>n <b>e</b> |

- Figure 34. Illustrations representing the (a) slow growing matrix grains and (b) a grain which may grow in an abnormal manner.
- Figure 35. Illustration of the random nature in which 115 the bimodal grain growth in this material occurred.

In rece
a great dea
temperature
research ha
dislocation
understand
inherently
microstruc

intermeta
temperatu
temperatu
composit

of interme

the B2 st

Prom

properti range be

ductilit

dramati

mode fr

[6].

has re

#### INTRODUCTION

In recent years intermetallic aluminides have received a great deal of attention due to their potential as high temperature structural materials. The majority of the research has, thus far, been devoted to the examination of dislocation reactions and micro-alloying in an effort to understand and improve the mechanical properties of these inherently brittle materials. The areas of texture and microstructure evolution have, however, started to receive more attention as their influence on the physical properties of intermetallics is realized.

Prominent among these intermetallic alloys is FeAl with the B2 structure shown in fig. 1. Like many other intermetallic materials its strong points are a high melting temperature and good oxidation resistance at high temperatures [1]. FeAl exists in the B2 structure over the composition range of 34 to 51at% Al [2]. The physical properties of FeAl vary considerably over this composition range being, hard and brittle at stoichiometry (50at%) with ductility increasing as the material becomes iron rich [1,3-5]. Micro-alloying with boron results in an equally dramatic increases in strength with a change in fracture mode from intergranular to transgranular at low temperatures [6].

Examination of the microstructures of these FeAl alloys has revealed they also can have a significant effect on the

material p

display su

material properties. Many of the ductility problems mentioned above are not present in single crystals which display substantial ductility at low temperatures [7,8]. Work by Baker and Gaydosh

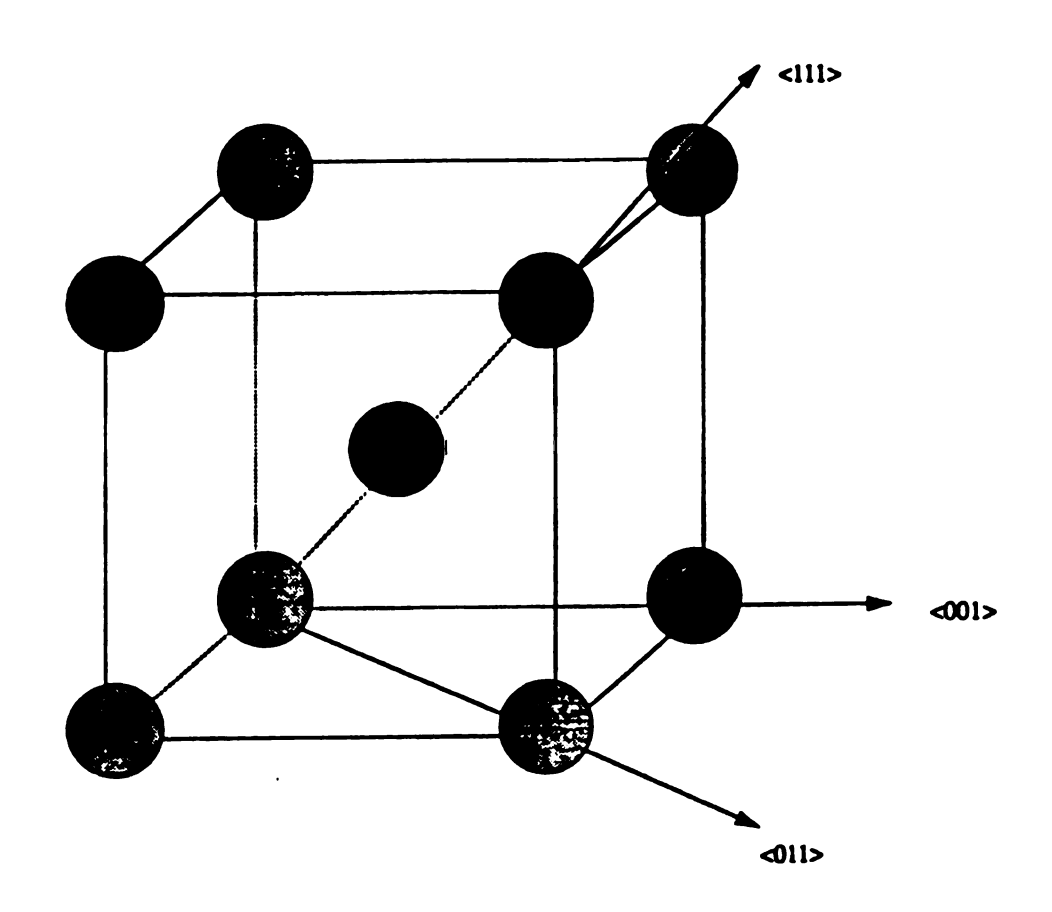


Figure 1. The unit cell of B2 FeAl alloys.

mittle trans melt spun rib iocumented si with changes alloyed powd boundary reg the material Bimoda: Well as a no growth is t grains in a then the ma of grain g as a small Mtrix. I Was observ texture (t to the hea growth. technique the other in micros physical

research

sensitiv

Yet, not

[9] has shown

[9] has shown a link between grain size and the ductile brittle transition temperature in FeAl hot extruded from melt spun ribbons. Earlier work by Whittenberger [10] documented significant variations in compression strength with changes in grain size in FeAl hot extruded from prealloyed powders. All of these studies suggest the grain boundary regions of these alloys may play a major role in the materials behavior.

Bimodal grain growth has also been observed in FeAl as well as a number of other intermetallics [3,11-14]. Bimodal growth is the phenomenon where a relatively small number of grains in a polycrystalline matrix grow much more rapidly then the majority of matrix grains. The result of this type of grain growth can be a completely different microstructure as a small number of grains will come to dominate the entire matrix. In at least one of these cases where bimodal growth was observed [3] the material possessed a significant texture (texture here meaning a preferred orientation) prior to the heat treat treatment which resulted in bimodal grain growth. Considering extrusion is one of the common techniques for production of these materials, it is likely the other materials were textured also. This type of change in microstructure can have a significant effect on the physical properties of any material and, as mentioned above, research on FeAl has already shown it to be microstructure sensitive. The reasons for bimodal grain growth are, as yet, not well understood. The purpose of this study is to

examine the relationship between texture and bimodal grain growth in B2 FeAl. But before the behavior of this material in particular can be examined a general review of the nature of grain growth should be undertaken.

#### GRAIN GROWTH

The primary driving force behind grain growth in a strain free crystalline matrix is the surface energy present at the grain boundaries [15,16]. Each grain boundary represents a interface and, therefore, has a certain amount of surface energy. To reduce the total surface energy of the matrix the grains will grow in size which reduces the total number of grains and, therefore, the total surface area of the grain boundaries. With a reduction of the total grain boundary area comes a lowering of the total surface energy.

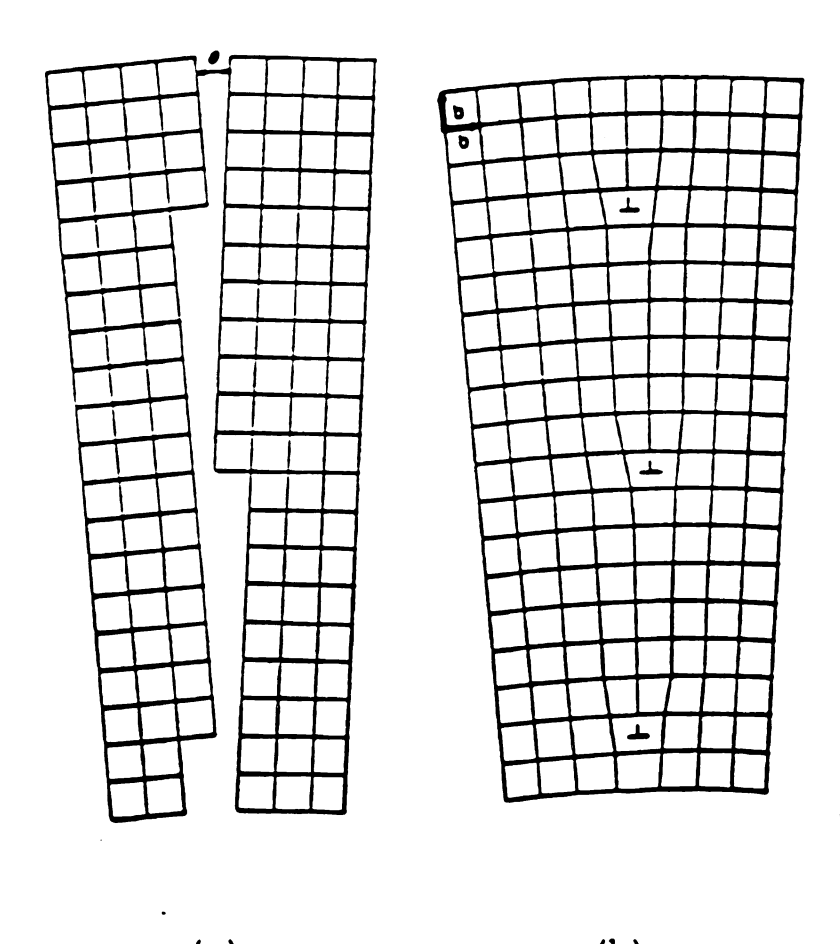
The rate at which grains are able to grow is dependent on how fast the grain boundaries can migrate through the crystalline matrix. The rate of grain boundary migration is a balance between the driving forces for migration and the barriers against it. To understand grain boundary migration, and the factors which influence it, the nature of grain boundaries must first be examined.

#### Grain Boundaries

There are five degrees of freedom which need to be considered when describing the geometrical relationship between two adjacent grains. Two define the crystallographic direction in the grains being compared (i.e. the direction of interest in the grains, like [001], or [111]), one to define the angle of misorientation between the above selected direction (i.e. the angle of rotation between the chosen directions in the grains), and another to define the boundary plane with respect to the crystal axis. When choosing the crystallographic directions of the grains, it is common to assume that the same direction in both grains is being considered since this is much easier to visualize. For the purpose of this study this convention will hold true.

either low angle or high angle boundaries depending on the relative misorientation of the adjacent grains. Low angle boundaries are considered to have misorientations up to approximately 10 degrees, with larger misorientations classified as high angle boundaries. The grain misorientation can be in the form of a twist or tilt, and boundaries with both components are not uncommon.

The accepted model for low angle boundaries is that of an array of dislocations as shown in fig. 2. When two adjacent grains are only slightly misoriented the boundary can be pictured as a stack of independent dislocations.



(a) (b)

Figure 2. Diagram of low angle symmetric tilt boundaries.

(a) How crystals may appear if separated. (b)

Dislocation structure after joining. [36]

This model has b behavior of low at angles of mis [15,17]. As th dislocations ar between their o this model is n High angle angle between region becomes normal lattice area. With th lattice posit: region increas forced out of in the bounda true nature c debate, and r this problem. the boundary energy for a explanation . migration an models and i expand the s into account

Which would

This model has been very successful in predicting the behavior of low angle boundaries, but starts to break down at angles of misorientation on the order of 10 degrees [15,17]. As the angle of misorientation increases the dislocations are soon so close together that the interaction between their cores significantly affects their behavior and this model is no longer valid.

High angle boundaries are less well understood. As the angle between grains increases the geometry of the boundary region becomes more complex as greater deviations from normal lattice positions are required to fill the boundary area. With these more drastic deviations from normal lattice positions, strain fields at and near the boundary region increase in density and intensity as more atoms are forced out of their normal lattice positions. This results in the boundary areas being a very complicated region. true nature of high angle grain boundaries is still open to debate, and researchers have taken two approaches to solving this problem. The first is to try and arrange the atoms at the boundary in such a way as to minimize the boundary energy for a given angle. This method provides a possible explanation for some unusual observations in grain boundary migration and has resulted in the coincidence site lattice models and its numerous extensions. The second is to try and expand the simple dislocation model discussed above to take into account the interactions of the arrays of dislocation which would result at high angle boundaries.

The Coinciden There is grain misorie behavior of a geometry of determining straight for about the st When th superimposed aisorientati both grains is illustrat are often re of common 1 (CSL's). T grains is d notation fo fraction of lattice pos the <111> notation i relationsh axis of rc The c boundarie: the late : The Coincidence Site Lattice Boundary

There is strong evidence that even small changes in grain misorientation can have significant effects on the behavior of a grain boundary [18-20]. This implies that the geometry of the boundary may play an important role in determining its behavior. This insight, while seeming straight forward, can lead to some important conclusions about the structure of grain boundaries.

When the lattice of two adjacent grains are superimposed upon one another there are certain angles of misorientation where a proportion of the lattice sites from both grains fall at the same point in space. This situation is illustrated in fig. 3 and these angles of misorientation are often referred to as "special" angles, with the points of common lattice sites called coincidence site lattices (CSL's). The proportion of lattice sites common to both grains is dependent on the angle of misorientation. notation for the CSL number is a  $\Sigma$  and the inverse of the fraction of common sites. For example, fig. 3 shows the lattice positions of two grains rotated 38.2 degrees about the <111> direction. They have 1 in 7 common sites so the notation is  $\Sigma$  7. Table I shows some common CSL relationships with the angle of misorientation for a given axis of rotation.

The concept of the coincidence site lattice at grain boundaries was first recognized by Kronberg and Wilson in the late 1940's. When two grains are in a coincidence

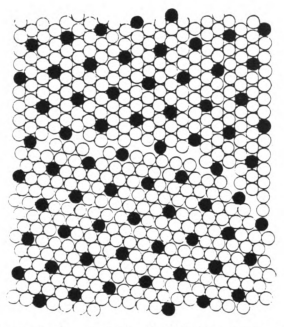


Figure 3. Two crystals rotated 38° to form a CSL relationship. The black dot represent the coincidence lattice common to both crystals [37].

Table 1. Angles of misorientation for various common CSL situations [48].

| Rotational axis | Σ      | Minimum        |
|-----------------|--------|----------------|
| <100>           | 5<br>5 | 28.1<br>36.9   |
|                 | 5      | 22.6           |
| <110>           | 3<br>9 | 70.5<br>38.6   |
|                 | 11     | 50.5           |
| <111>           | 3      | 60.0           |
| <211>           | 7      | 38.2<br>180.0  |
|                 | 5      | 101.6<br>135.7 |
| <311>           | 3      | 146.4          |
|                 | 9      | 67.1           |

relationship t atoms on these either grain. as to why cert my result in There have si boundaries at have special mobilities ar initial CSL m angle grain ) some specifi The coi Bishop and C site model t angles, and above, the idea that a grains will these commo Misorientat important p boundary. special and <sup>adjustment</sup> <sup>com</sup>pensate allows the relationship the grain boundary between the grains will have atoms on these coincidence sites which belong equally to either grain. The model was used as a possible explanation as to why certain angles of misorientation between grains may result in grain boundaries with unusual properties.

There have since been numerous studies which have shown boundaries at or near these special misorientation angles to have special properties such as higher than average mobilities and lower than average energy [18,21-24]. This initial CSL model is not, however, a complete model of high angle grain boundaries, but it does a good job of explaining some specific phenomenon which have been observed.

The coincidence site model was taken a step further by Bishop and Chalmers [25]. Starting with the coincidence site model they extended it to angles near the special angles, and then to all angles in between. As explained above, the coincidence site lattice model is based on the idea that at special angles of misorientation adjacent grains will share common lattice sites. The frequency of these common lattice sites depends on the angle of misorientation. Bishop and Chalmers suggested that a more important parameter is the coincidence sites at the boundary. At angles of misorientation slightly off these special angles Bishop and Chalmers propose that a periodic adjustment in the boundary structure, as shown in fig. 4, to compensate for the imperfect fit of the lattice. This allows the boundary to maintain a coincidence relationship

while the lattic[ every N coincide bundary structu special angle ge becomes more rem mrrections beco between two spec This idea w [26] when they p grain boundary not an exact co coincidence rel relative shift of repeating st regardless of boundary. Cha small unit of opposed to the allows for th region to pos simulations ( Deviation handled in t Chalmers. N alternating <sup>symmet</sup>rical

repeated so

while the lattice does not. The result is a boundary where every N coincidence sites there is an adjustment in the boundary structure to account for the deviation from the special angle geometry. As the angle of misorientation becomes more removed from a special angle the periodic corrections become more frequent until a point half way between two special angles where the misfit is a maximum.

This idea was further modified by Chalmers and Gleiter [26] when they proposed that the important feature of the grain boundary is the periodic nature of the structure and not an exact coincidence fit. Fig. 5 shows (a) an exact coincidence relationship with shared atoms while (b) shows a relative shift in the lattice positions. The smallest unit of repeating structure is of length 'p' in both cases regardless of whether there are shared atoms in the boundary. Chalmers and Gleiter suggest that it is this small unit of repeating structure which is of importance as opposed to the shared atoms at the boundary. This idea also allows for the relaxation of the atoms in the boundary region to positions of lower energy which recent computer simulations [27,28] suggest would happen.

Deviations from the special angles of exact fit are handled in the same manner as the model by Bishop and Chalmers. Non-symmetric boundaries are formed by alternating the structural units between the two nearest symmetrical planes. The small units are alternated and repeated so that the correct average angle results.

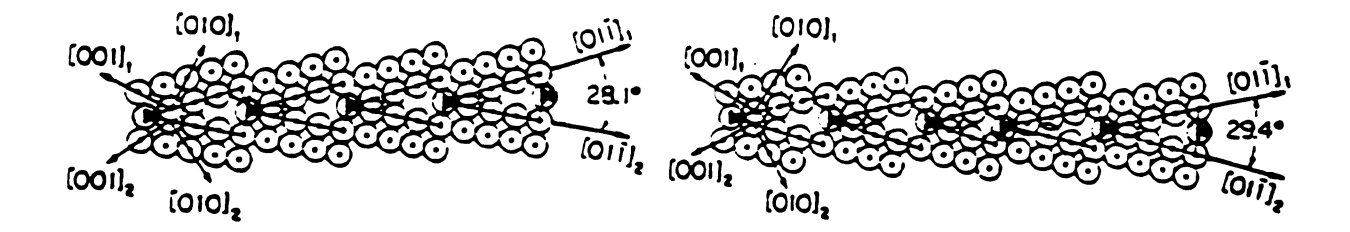
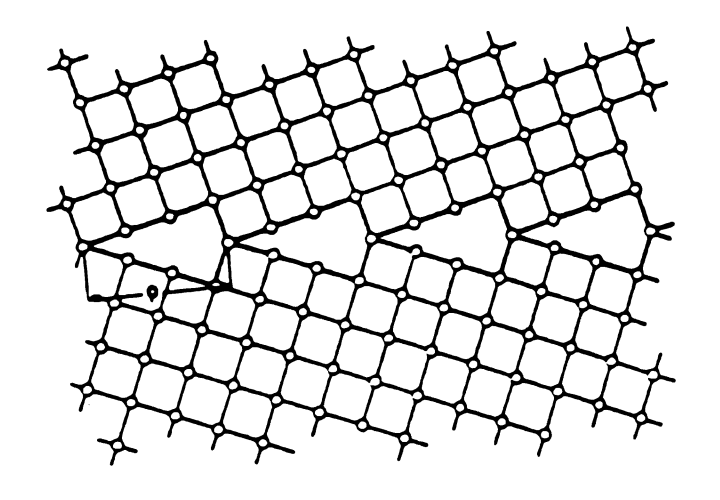
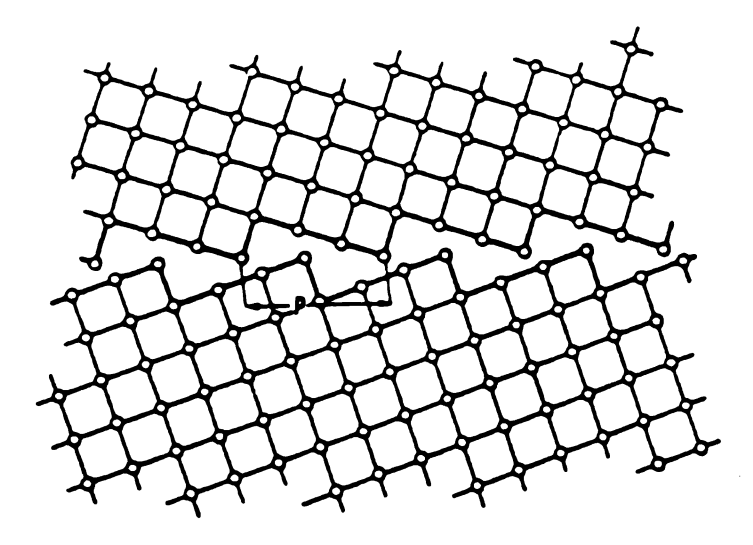


Figure 4. Periodic adjustments at grain boundaries as described by Bishop and Chalmers [25].





(a)



(b)

Figure 5. (a) 37° <001> tilt boundary. The lattices are placed so that the lattice sites are shared in the boundary. (b) The same 37° <001> tilt boundary with the two crystals displaced so no lattice positions are shared [26].

The Dis

disloc

R

early bounda

dislo

formed

lisor

is fo

bound

and b

dislo sugge

case

tilt

EXSI

degr eith

gCC(

роп

str red

dis

cot

e];

The Dislocation Boundary

Read and Shockley were the first to propose a dislocation model for high angle grain boundaries in the early 1950's. Limiting their model to symmetric tilt boundaries, they assumed that by uniformly distributing the dislocations in the interface, a low energy boundary is formed. There are, however, only certain angles of misorientation where a uniform distribution of dislocations is formed. Fig. 6 shows a) a symmetric 53 degree tilt boundary, where the dislocations are uniformly distributed and b) a symmetric 60 degree tilt boundary, where the dislocations do not form a uniform boundary. The model suggests that non-uniform boundaries, like the 60 degree case, are made up of uniform boundaries plus small angle tilt boundaries to compensate for the deviation. For example, the 60 degree boundary could be made with a 53 degree uniform boundary plus two 3.5 degree boundaries on either side. This model, however, does not take into account the effects of elastic interaction between the boundary dislocations.

Marcinkowski and Jagannadham [29,30] proposed that the structure of the boundary region is a compromise between reducing voids at the interface and minimizing elastic distortion. Figure 7 shows three possible boundary configurations. Figure 7(a) shows a boundary with no elastic distortion in the lattice but void space at the

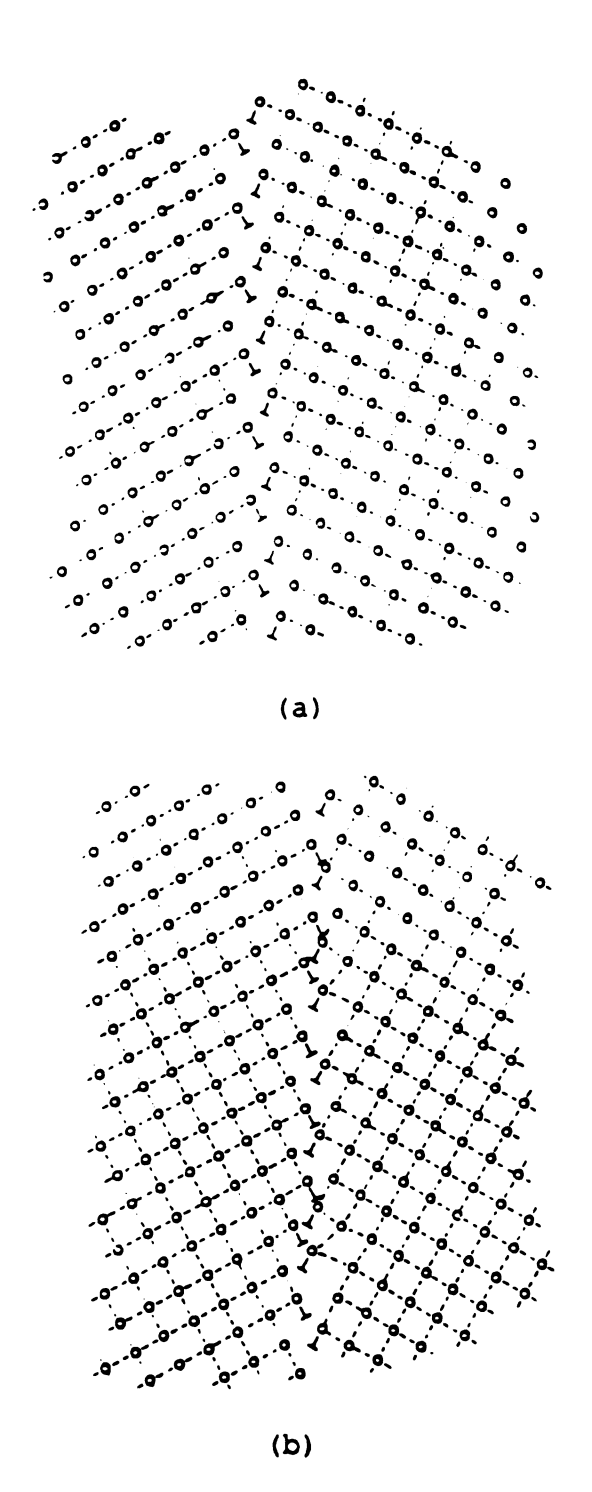


Figure 6. (a) Dislocation model of a 53° symmetric tilt boundary. (b) Dislocation model of a 60° symmetric tilt boundary [37].

boundary is at a maximum which means a high surface energy, fig 7(b) shows a boundary with some elastic distortion but much less void space then (a), while fig 7(c) shows the elimination of void space but the maximum of elastic distortion. Marcinkowski and Jaganndham showed the situation illustrated in fig. 7 (b) to be the likely case for real crystals. It is also shown that the surface of the voids in the partially coalesced model is not stress free and there is an array of very weak dislocation dipoles distributed across the surface. Figure 8 shows the boundary in the partially coalesced case with the dislocation dipoles at the void surfaces and an array of dislocations a short distance from the interface to screen their stress fields. The equilibrium configuration is obtained by minimizing the sum of the surface energy associated with the voids and the energy contained in the stress fields.

The Marcinkowski and Jagannadham model treats non-uniform boundaries very differently then does the Read and Shockley model discussed previously. This model suggests that non-uniform boundaries are made up of non-uniformly distributed dislocations. Again there are voids and regions of coalescence, only in this model they are not evenly distributed. This results in non-uniform stress fields along the boundary which repeat with a period dependent on the angle of misorientation. As with the uniform boundary the equilibrium configuration is achieved by minimizing the total energy.

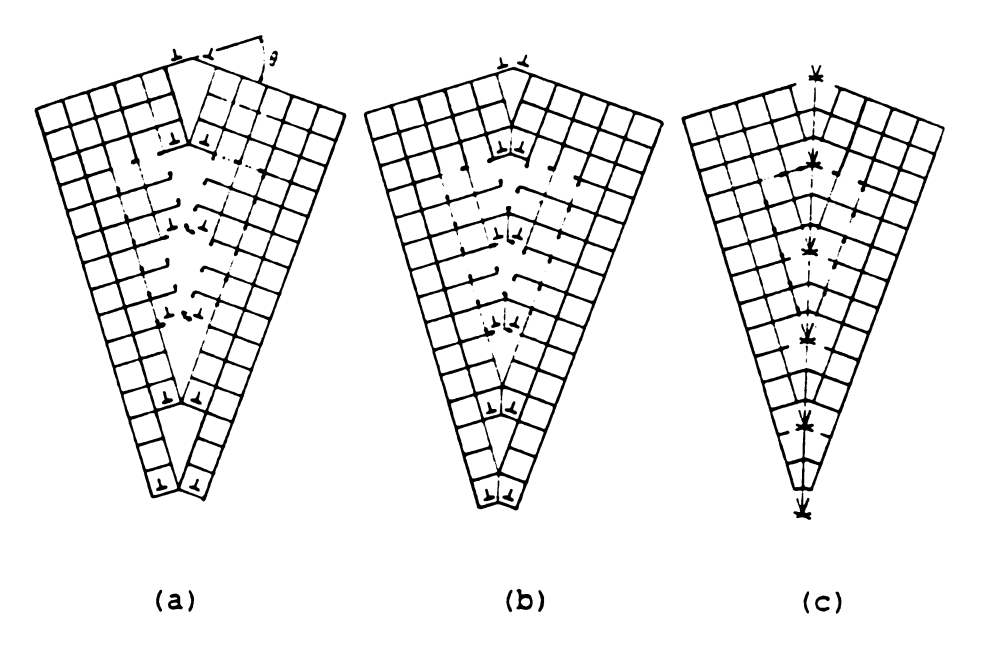


Figure 7. (a) A boundary with no coalescence, (b) partial coalescence, and (c) total coalescence [30].

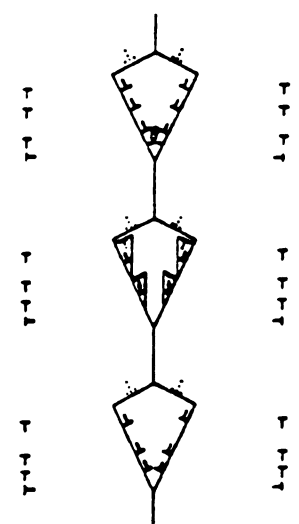


Figure 8. Partially coalesced boundary with an array of dislocations screening the boundary from the matrix [30].

### Summary

Though many of the details of these various theories differ, the basic idea of a repeating structure appears in almost every one. Boundaries between grains with special angles of misorientation have small repeating structures of good fit while boundaries between grains with non-special misorientations have regions of good fit followed by regions of poor fit.

### Grain Boundary Energy and Mobility

### Grain Boundary Migration

An accurate description of grain boundary migration requires an understanding of the grain boundary structures. As discussed, our understanding of grain boundary structures is less then perfect. This places serious limitations on our ability to describe boundary migration, especially when there is evidence that a moving boundary may be different from static ones [31]. Still, there are models available for boundary migration and the following section will be a brief outline of the more prevalent.

#### Dislocation Migration

Based on the dislocation model for grain boundary structures, grain boundary migration can be modeled using dislocation glide and climb mechanisms. For low angle

boundaries it has been experimentally shown [32,33] that the boundaries can be made to migrate by applying a stress to the material, and the direction of migration can be reversed by reversing the direction of the applied stress. From this and evidence that the migration rates increase with increased temperature and decrease with increasing misorientation [32,33], it has been generally accepted that dislocation glide is the mechanism for low angle grain boundary migration.

Migration of high angle grain boundaries using dislocation theory is considerable more complicated. With the exception of special angle boundaries [20,34], whole networks of dislocations must move to facilitate boundary migration. This requires dislocation glide and climb, as well as diffusionless atomic shuffles to produce migration. Boundaries between grains of special angles of misorientation require only glide for migrations.

#### Vapor Mechanisms

Gleiter [31] proposed a theory where individual atoms jump from a grain into the boundary region where they can then make several more jumps before reattaching to a grain, be it the original grain or the neighboring grain. Grain growth occurs when there is a flux of atoms in the boundary is favoring one grain over another. Gleiter related the process to grain growth by vapor deposition where the growing grains are built up by atoms being deposited on

ledge type structures. This model allows the atoms in the boundary region to move about very easily, almost as if they were in a vapor phase.

#### Diffusion Mechanisms

If the boundary region is viewed as being narrow, with "narrow" being up to several atomic spacings, it is conceivable that the atoms may jump the gap in one step. The result would be a diffusion type mode of boundary migration. This idea was examined in detail by Lucke, Rixen, and Rosenbaum [35]. Figure 9 shows a free energy diagram for a atom crossing a narrow boundary in one step. The solid line representing a stationary boundary where the activation energy is the same for a jump in either direction. The dashed line represents a boundary where the activation energy going from right to left is higher then going from left to right. This situation favors diffusion from left to right and therefore boundary migration from right to left.

Lucke, Rixen, and Rosenbaum [35] derived an equation for the velocity of boundary migration based on free energy differences and activation energies. If in the situation seen in fig. 9 the activation energy in one direction is g/2 more then the average activation energy and in the other direction g/2 less then average, the following equation for the boundary velocity is obtained.

where; D = diffusion constant,

y = (D g/bkT) exp(-H/kT) g = free energy of activation,

b = atom spacing,

H = enthalpy,

This equation holds for g << kT which is true for grain growth and recrystallization. When comparisons were made between calculated and experimentally measured boundary velocities the equation seemed reasonable for materials of very high purity. However, it was found that even very small amounts of impurities can result in large changes in both the diffusion constant D and activation energy H. It was reasoned this was due to the segregation of impurity atoms to the boundary. Impurities in the boundary cause a decrease in the diffusion constant and increased activation energy, both of which slow boundary migration.

In the same paper these authors describe the motion of boundaries with impurities present. Their 'Impurity Drag Theory' describes the moving boundary as having an 'atmosphere' of foreign atoms lagging behind the boundary exerting a drag on the moving boundary. They also suggest that at sufficiently high boundary velocities, (i.e. sufficiently high temperatures) the boundary may break away from impurity atoms and not drag them along as they move. This results in boundary velocities similar to those expected in very pure materials. The boundary motion under these conditions becomes considerably more complicated.

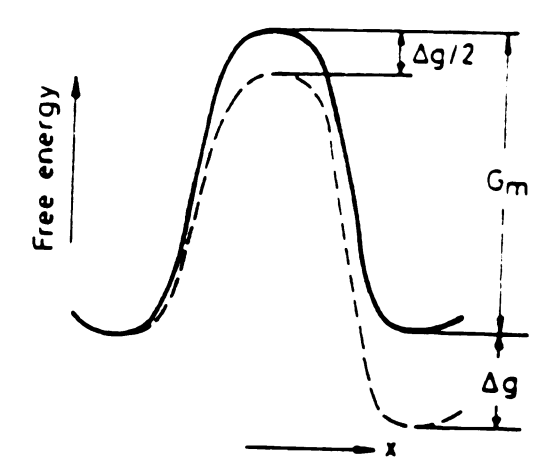


Figure 9. The free energy diagram of an atom crossing a narrow grain boundary [35].

# Orientation Dependence of Migration Rate

Thus far, no mention has been made about how boundary geometry may effect the behavior of migration. Recalling the various theories on boundary structures it was pointed out that when certain angles occur between grains special geometries may be set up at the boundary. These geometries correspond to angles of 'good fit' at the boundary. At

these angles of good fit low energy boundaries are formed [36,37,38]. For boundaries formed between grains at or near special angles of misorientation unusual grain boundary behavior has been observed [18,39].

Aust and Rutter [18] were among the first to do extensive research into this phenomenon. Using bicrystals of zone refined lead, Aust and Rutter examined the effect orientation has on boundary migration. They examined the differences in migration rate between boundaries of random orientation and special boundaries with misorientation angles near 23 and 40 degrees about the <111> directions and 28 degrees about the <100> direction. The driving force for migration was provided by a striation substructure in the single crystal which was to be consumed. The striations are a form of sub-boundary formed during the growth process of the single crystals which represent a reproducible concentration of dislocations. High purity lead with controlled amounts of tin was used to examine the influence soluble impurities may have on boundary migration. Figures 10 and 11 show some of the results of their experiments. If the line for special angle boundaries in fig. 10 is extended back to extremely high purity, it appears that the migration rate for all boundaries is approximately the same. However, as the concentration of tin is increased the special angle boundaries clearly migrate faster then random boundaries. Correspondingly, fig. 11 shows that as the activation energy for random

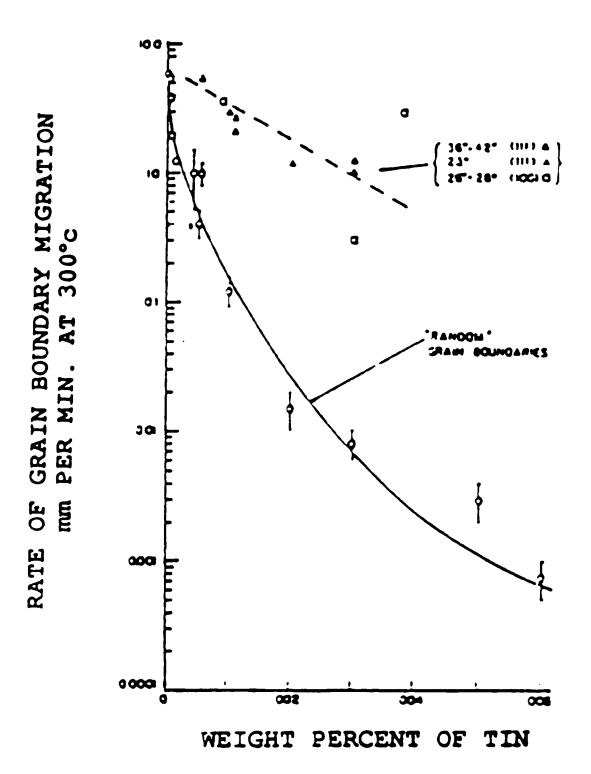


Figure 10. Rate of boundary migration at 300°C as a function of tin concentration in zone refined lead, for random and special angle boundaries [18].

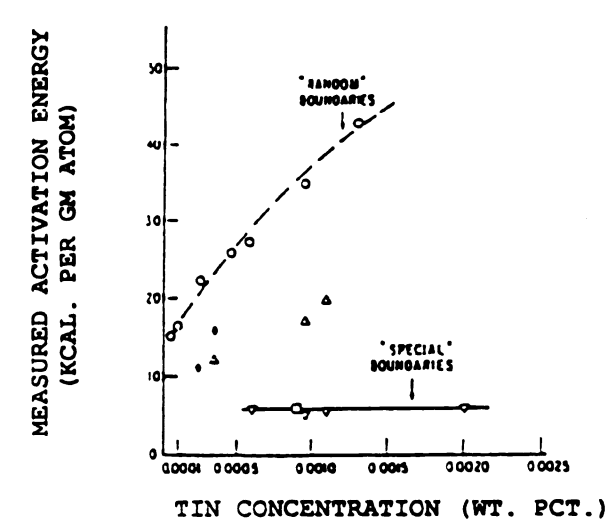


Figure 11. Activation energy for boundary migration as a function of tin concentration in zone refined lead for random and special angle boundaries [18].

boundaries increases with increased tin content, the tin concentration has little effect on the activation energy for special boundaries. Aust and Rutter suggest these results may be explained with the CSL model for boundary structure. If the boundaries have a 'good fit' impurities would be less likely to segregate there. Therefore, with little or no drag from impurities on CSL type boundaries, these boundaries would be free to migrate at a normal rate while non-CSL type boundaries would be slowed by impurity drag.

When Kronberg and Wilson originally put forth the CSL model for grain boundaries they suggested that the boundaries of high coincidence site density would be high mobility boundaries. The idea was that since the boundary has a 'good fit' the boundary region would be narrow so the jump distance for atoms would be short. Atoms on the coincidence sites would move very little, if at all, and the other atoms with only short jumps would require lower activation energies. The concept of lower activation energy for shorter jumps intuitively sounds reasonable but may not be enough to justify high mobility grain boundaries. As pointed out by Gordon and Vandermeer [19], if a boundary is in exact CSL conditions it will be a very ordered region and a highly ordered matrix tends to reduce diffusion rates since there is little porosity and few vacancies. Thus they reasoned exact CSL conditions would not increase boundary migration rates. Gordon and Vandermeer used the example of coherent twin boundaries which are known to have very low

mobilities, but which are also symmetric CSL boundaries with the highest number of shared atoms at the boundary.

As a possible solution to this apparent contradiction Gordon and Vandermeer [19] suggest it is not the exact CSL boundaries but boundaries near CSL relationships which have high mobility. These near CSL boundaries would still be ordered, thereby reducing the segregation of impurity atoms to the boundary, but now contain some dislocations which would introduce porosity to aid diffusion. Lucke, Rixen and Rosenbaum [35] agree that exact CSL boundaries may not be the high mobility boundaries and went on to show that grains possessing near but not exact CSL relationships displayed preferred growth in a rolled aluminum single crystal.

#### Summary

The motion of grain boundaries is, quite naturally, closely related to the structure of the boundary in question. Generally speaking, the mechanism for low angle boundary migration is dislocation glide which produces a correspondingly low rate of migration. Migration of high angle boundaries is much more complex as the mechanisms for migration are still not clear. Large variations in migration rates are seen with relatively small changes in boundary angle or impurity content. High rates of migration are often seen for boundaries with angle at or near special CSL angles which produce boundaries where the atom position are fairly well ordered. Away from CSL angles the

boundaries become very disordered regions and migration slows. The mechanism of high angle boundary migration, whether it be a dislocation mechanism, atomic diffusions or diffusionless atomic shuffles, is still a matter of debate.

#### Grain Growth

To discuss grain growth in general we need only apply the grain boundary migration theories to polycrystalline materials. Normal grain growth is expected and seen in most non-textured, fully dense materials with normal grain structures. In this type of material there is a random distribution of grain boundary angles and sizes so there are no large advantages or disadvantages for any grains during grain growth. The result is a shift to larger average grain sizes but little change in grain size distribution as grain growth proceeds.

Bimodal grain growth can occur when some group or type of grain has some advantage in grain growth over the rest of the matrix. During bimodal grain growth a small number of grains grow at a much faster rate then the surrounding matrix. The result is relatively few grains grow to dominate the entire matrix, often producing unusually large grains in the process. There are now two commonly accepted situations which can result in bimodal grain growth. First, if for some reason there is a small number of relatively large grains surrounded by a matrix of smaller grains the

larger grains will have an advantage during grain growth due to grain boundary curvature. Recent studies, however, indicate that grain boundary curvature alone may not be sufficient to trigger abnormal grain growth [40,41]. Worner and co-workers [40] show that if the grain growth of the matrix grains is slowed by a dispersion of pinning particles bimodal grain growth can then occur. The theory states that the larger grain can more easily overcome the pinning effects of the particles. This conclusion is supported by computer simulations done by Srolovitz and co-workers [42].

The second situation which may lead to bimodal grain growth involves materials that have a crystallographic texture, texture here meaning there is a strongly preferred orientation common to the majority of the matrix grains. The theory is based on differences in grain boundary mobilities due to variations in grain boundary orientations, as discussed in previous sections. Computer simulations have shown that a small number of grains possessing grain boundaries with high mobility may grow in an abnormal fashion if they are surrounded by a matrix of grains with low mobilities [43]. In this situation theoretical work suggests unusually large grains are not needed to initiate abnormal growth [44], since the advantage in grain growth comes from the grain boundary mobility, not grain boundary curvature or energy. This is thought to be the situation in textured materials which display bimodal growth. Most grain boundaries in highly textured materials are low angle

boundaries and therefore have low mobilities [18,45]. If grains are present in this highly textured material which have orientations that differ significantly from those of the matrix grains their boundaries will be high angle boundaries and therefore have higher mobilities. This results in a growth rate for these grains which can be significantly higher then the matrix grains.

#### Recrystallization

For the purpose of this study recrystallization will imply the process of grain growth to reduce the strain energy in a deformed matrix. During dynamic recrystallization both deformation and recrystallization are occurring simultaneously in a material. This results in a very complicated set of mechanisms acting at the same time in a small local area. The process of deformation is resulting in increased dislocation concentrations leading to pile ups and strain hardening, while recrystallization is annihilating dislocations and creating strain free grains. The mechanisms involved in deformation and strain hardening have been extensively studied elsewhere and shall only be mentioned when they have a direct bearing on the resulting microstructure and texture. The theories behind the mechanisms for nucleation and recrystallization, however, have a direct influence on the resulting microstructure and texture and so are of interest.

Recrystallization begins with the nucleation of new

crystals. Nuclei are formed at elevated temperatures where dislocations and other crystal imperfections can migrate to lower energy configurations forming subgrain boundaries surrounding relatively strain free subgrains. Subgrains can then become nucleation sites under the right conditions. The subgrains most likely to develop into nuclei tend to be in the areas of highest local deformation, like grain boundaries and second phase particles [46,47,48]. Subgrains which reach a certain minimum size, which varies with the surrounding microstructure, will then come under the influence of the normal driving forces behind grain growth. Prior to this point the subgrain boundaries are driven primarily by dislocation mechanisms [46,48]. Once this stage is reached the subgrain becomes a nucleus for a new grain and if the conditions are favorable in the surrounding matrix the nucleus will grow into the strained matrix and recrystallization can proceed.

Once a nuclei is formed, recrystallization is controlled by the driving forces for grain growth in the newly created grains. The energy source for grain growth in dynamic recrystallization is the difference in the density of dislocations between the growing grains and the deformed matrix. In the early stages of recrystallization the nuclei and new grains have very low dislocation densities so there is a large energy difference across the grain boundary to the deformed matrix which has a relatively high dislocation density. This provides a large driving force for grain

growth. As deformation proceeds the growing grains are deformed and start to accumulate significant numbers of dislocations. This reduces the driving force for grain growth and therefore the speed. When the density of dislocations within the growing grains becomes too great the energy difference across the boundary will drop below what is needed to drive grain boundary migration and grain growth will stop. This cycle of nucleation and grain growth to termination may repeat itself many times during a single hot deformation depending on numerous factors such as the amount of deformation, the temperature, or the material.

The development of a preferred orientation during deformation is very common. Recrystallization of a textured material quite naturally may result in a material which is again textured though not necessarily possessing the same texture [46,49,50]. During dynamic recrystallization a material is being deformed, resulting in a texture, at the same time recrystallization is taking place. Which of these two processes is the dominating factor, however, is still in question. There are two schools of thought on the development of textures during dynamic recrystallization, one being that of oriented nucleation proposed by Burgers [51] and the other being oriented growth proposed by Beck [52].

The theory of oriented nucleation states that in a deformed textured matrix there is a preference for nucleation in a particular crystallographic orientation.

These oriented nuclei then grow to form the new matrix with their orientation. The theory of oriented growth states that in a deformed matrix nuclei are so numerous that all orientations are present, but only those with orientations advantageous to grain boundary migration are able to grow. These grain will then form the new matrix with their preferred orientation. Today it is generally believed that a combination of the two theories is needed for a complete picture. Both mechanisms will contribute to the recrystallization behavior, with the processing conditions determining the dominating factor.

#### Texture and Grain Growth in FeAl

Previous studies on FeAl and similar nickel-aluminides [53] have shown significant texturing to occur during production of the material. Hot extrusion of Fe-40at%Al pre-alloyed powders at 977° C with a 16:1 reduction ratio resulted in material with a <111> wire texture [53]. In contrast, Fe-40at%Al hot extruded from cast billets at the identical temperature and extrusion ratio did not produce a <111> wire texture but instead a <110> wire texture was observed [53]. The reason for this difference in texture between cast and powder processed material in FeAl is unclear though it is apparently related to the materials pre-extrusion condition. Similar processing of NiAl alloys resulted in a <111> wire texture for both cast and powder processed material [53].

re to ex ir [1 si Da sto 90( ric

٧

<

D

g:

4 (

gi

at

- of

Ver

Hot extrusion of Fe-47at%Al melt spun ribbons at 977° C with a 16:1 reduction ratio also resulted in material with a <111> wire texture [9,54]. Upon heat treatment of this material for 5 hrs. at 1200° C there was an increase in grain size from 16 to 27 microns. Hot extrusion of Fe-40at%Al powder at 923° C produced material with an initial grain size of 9 microns grew to only 11 micron after 16 hrs. at 1023° C, while the same material extruded at 1227° C resulted material with a grain size of 55 micron which grew to 185 microns after 16 hrs. at 1257° C [10]. Grain growth experiments of multiply extruded ingots of FeAl of various iron to aluminum ratios showed several interesting points [1]. First, the rate of grain growth appears to vary significantly with the iron/aluminum ratio. Iron rich materials exhibited higher grain growth rates then did stoichiometric or slightly aluminum rich material at both 900° C and 1200° C. And second, at 900° C, only the iron rich material showed significant growth while at 1200° C all of the material displayed rapid grain growth rates which were several times those seen at 900° C.

#### PROCEDURE

#### Materials

All the materials examined in this study were Fe-40at%Al with the exception of one series of Fe-50at%Al. Small additions of boron were made to some of material to examine its effects on the materials properties. Complete chemistries can be found in table II. The materials were produced by hot extrusion of pre-alloyed powders or hot extrusion of cast billets. The first series of bars was produced by a single hot extrusion of pre-alloyed powder at 977°C to an area reduction of 16:1. The second series was produced by a double extrusion of pre-alloyed powders with the first extrusion at 977°C and area reduction of 8:1, and the second extrusion at 1077°C with are reduction of 6:1. The third series was produced from a cast ingot which was then extruded at 977°C with area reduction of 16:1. All heat treatments were performed in flowing argon for 24 hours. The forth series was a double extrusion of prealloyed powders with the first extrusion at 977°C and area reduction of 8:1, and the second extrusion at 800°C and area reduction of 6:1. The extrusions were performed at the NASA Lewis Research Center in Brookpark, Ohio (See appendix I for further details on the extrusion process).

Table II. Chemical analysis of FeAl alloys after extrusion [3].

# Material Compositions (weight %) Powder Processed Material

| Material                                     | Al    | Co   | Cr   | Mn   | Ta  | N      | 0     | В    | Fe  |
|--|-------|------|------|------|-----|--------|-------|------|-----|
| Single extruded 16:1 reduction ratio         |       |      |      |      |     |        |       |      |     |
| Fe-40at%Al                                   | 25.03 | -    | -    | -    | -   | 0.0006 | 0.028 | -    | Bal |
| Fe-40at%Al+0.1B                              |       | -    | -    | -    | -   | W      | 11    | 0.10 | Bal |
| Double extruded 8:1 then 6:1 reduction ratio |       |      |      |      |     |        |       |      |     |
| Fe-40at%Al                                   | 24.4  | 0.08 | 0.1  | 0.1  | 0.3 | 0.004  | 0.061 | -    | Bal |
| Fe-40at%Al+0.2B                              | **    |      | •    |      | **  | **     | 0.066 | 0.19 | Bal |
| Fe-50at%Al                                   | 32.8  | -    | 0.02 | 0.01 | _   | 0.002  | 0.058 | -    | Bal |

# 

| Material        | Al      | H       | C            | P     | N      | 0      | В    | Fe  |
|-----------------|---------|---------|--------------|-------|--------|--------|------|-----|
| Single extruded | 16:1 re | duction | <u>ratio</u> |       |        |        |      |     |
| Fe-40at%Al      | 22.8    | 0.0002  | 0.0154       | 0.003 | 0.0003 | 0.0005 | -    | Bal |
| Fe-40at%Al+0.1B | 22.9    | 0.003   | 0.0214       | 0.001 | -      | 0.0009 | 0.13 | Bal |

#### Sample Preparation

Sample preparation for x-ray analysis consisted of sectioning the specimens to expose the desired surface and then grinding to 600 grit and metallurgically polishing.

Once polished and cleaned the samples were ready for examination.

For optical and scanning electron microscopy the polished specimens were etched with a solution of 100 parts water, 20 parts HNO<sub>3</sub>, 3 parts HF, and 2 parts HCl.

Grain sizes were determined with the following formula which is the line intercept method:

Grain Size = 
$$\frac{L}{M * N}$$

where: L = the length of the test line,

M = the magnification,

N = the number of intersections.

The lines were drawn randomly across the micrographs so nonequiaxed grains would not bias the results.

## X-ray Analysis

X-ray texture analysis was performed on a Scintag XDS 2000 x-ray diffractometer with pole figure goniometer. Pole figures were created from back reflected x-ray data, gathered through 360° rotation about the plane normal and zero to 70° tilted from the normal. Data was taken at 5° intervals in both the rotational and tilt directions. Once the data was collected the popLA [55] software was used to

gener inver

figur

compi

volt

sho:

pro

pea

and ind

The i

spac:

Plana

generate the pole and inverse pole figures. To generate the inverse pole figures the data from three independent pole figures were combined by the software to produce a more complete picture of the texture.

Copper k alpha radiation under a 40 kV accelerating voltage was used for all of the x-ray analysis. The first step was to run a normal diffraction pattern to locate the two theta positions of the planes of interest. Figure 12 shows a typical diffraction pattern from the powder processed FeAl. The set of planes which corresponds to each peak was determined using the Bragg equation,

Bragg Equation

$$\lambda = 2d * \sin(\theta),$$

where:

 $\lambda$  = the wavelength,  $\theta$  = the diffraction angle, d = planar spacing.

and the following equation relating planar spacing to Miller indices;

$$d = \frac{a}{(h^2 + k^2 + 1^2)^{1/2}}$$

where: d = the planar spacing, a = the lattice constant,

h,k,l = the Miller indices.

The Bragg equation is used first to calculate the planar spacing corresponding to each diffraction peak. These planar spacings are then used to determine the Miller

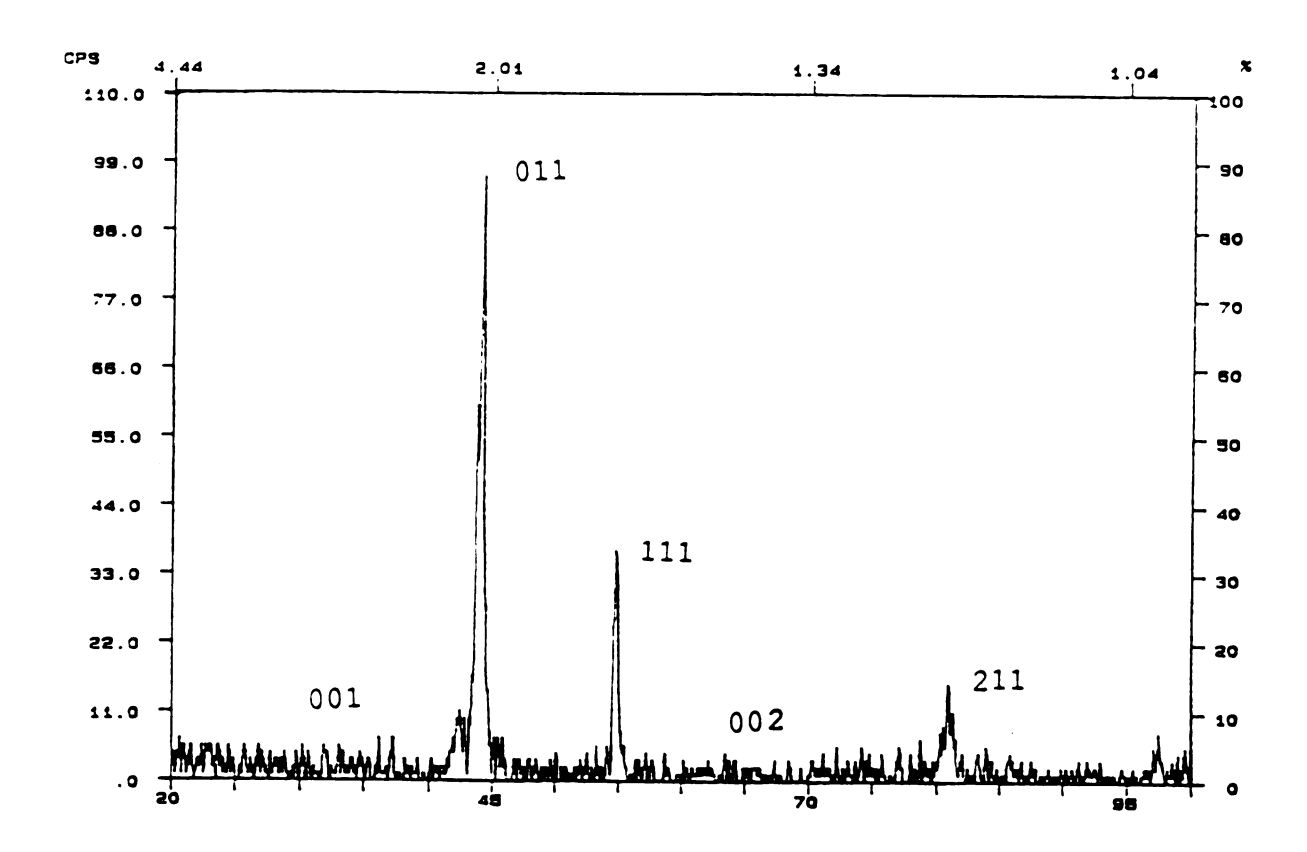


Figure 12. Diffraction pattern of FeAl alloy produced from powder processing using Cu  $\,k\alpha$  radiation.

pattern the diffraction angles were determined for specific planes. Pole figures were then taken on the (110), (111), and (211) families of planes. The (110) and (211) planes were chosen because they gave the highest x-ray intensities and the (111) planes were used because they were the planes of the most interest. This data was then used to generate inverse pole figures as mentioned above.

#### EBSP Analysis

Since Electron Backscatter Patterns (EBSP) are a relatively new development in the field of electron microscopy a short description of the processes is in order. Developed by Venables and coworkers [56] the technique uses Kikuchi lines [57] formed by backscattered electrons in an SEM to determine crystallographic information. Figure 13 shows a diagram of the EBSP set up. The normal rastering of the electron beam in the SEM is stopped and the beam is fixed on the area of interest. The surface to be examined is tilted so the incoming electron beam hits the surface at a steep angle. This is done to increase the intensity of backscattered electrons. Figure. 13 illustrates that a high tilt angle reduces both the amount of deflection and the escape distance needed for electrons leaving the specimen surface, resulting in an increase in the total number of electrons available to produce a pattern.

As the electron beam enters a specimen a continuous

# Incoming beam of electrons.

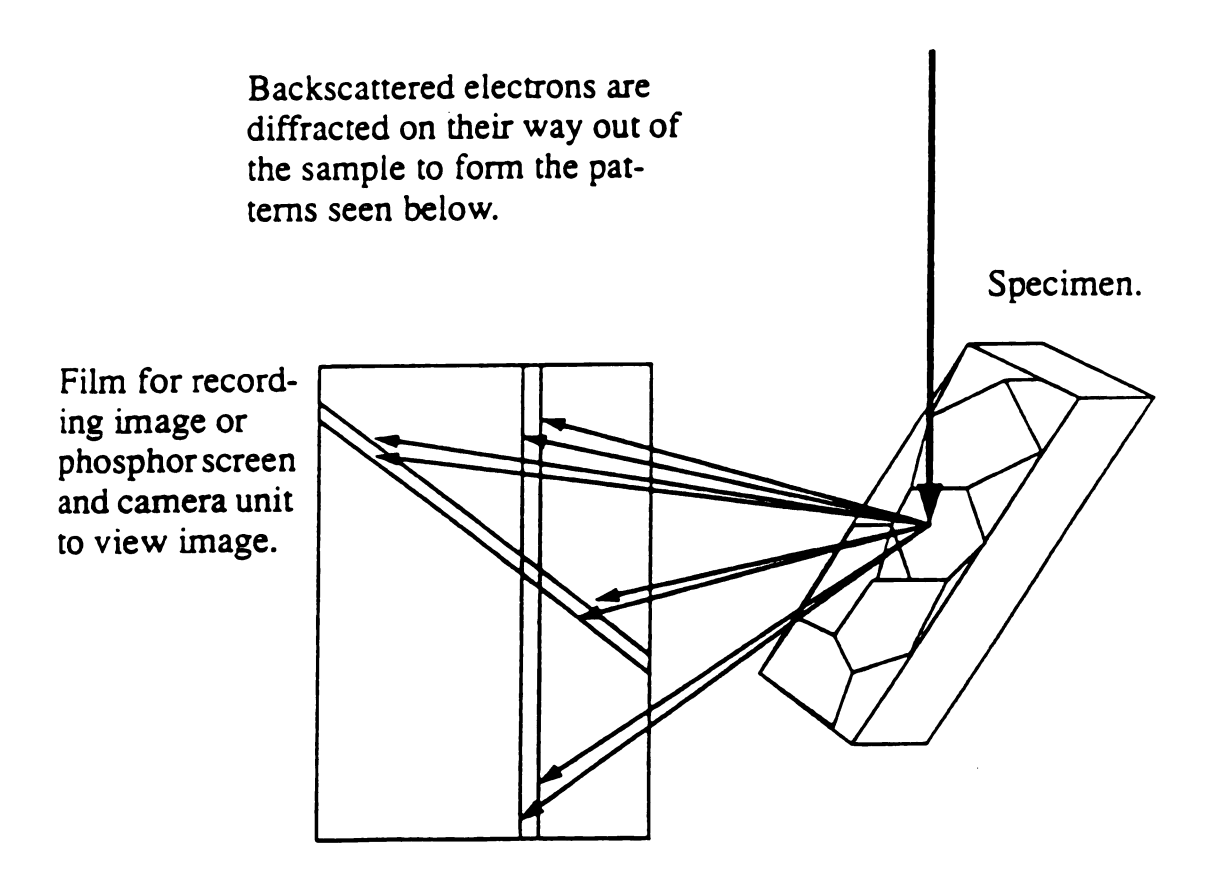


Figure 13. Illustration of the set up used to produce EBSP images.

shower of inelastically scattered electrons is formed and spreads out in all directions in the specimen. The pattern is formed as these elastically scattered electrons are Bragg diffracted on their way out of the sample. The atomic planes are bombarded from all directions by scattered electrons with a continuous range of energies. produces Bragg diffraction on all diffracting planes simultaneously so all the lattice planes contribute to the pattern. The Bragg diffraction produces cones of increased electron intensity where the diffracted electrons add to the randomly scattered back ground, and decreased electron intensity where the electrons are diffracted from their normal path. On a two dimensional phosphor screen or piece of film the cones form hyperbola bands where they intersect the flat surface. The patterns resulting from this phenomenon are called kikuchi patterns and are commonly used in transmission electron microscopy. The kikuchi patterns can be used to determine the orientation of the crystal producing the pattern as the location of the lines and zone axises are dictated by the orientation of the crystal lattice and the geometer of the system.

The electron backscatter patterns for this work were generated in a Hitachi 2500 SEM with 20 kV accelerating voltage and rear mounted TV camera for observation of the patterns. A phosphor screen is placed 40 mm from the sample inside the vacuum chamber. Just behind the phosphor screen a special low light TV camera is mounted to view the images

formed on the phosphor screen by the scattered electrons. The samples were tilted to 70° from horizontal so the beam struck the specimen at a 20° angle at a working distance of 11mm. The camera feeds the patterns to a CRT which is controlled by a Link AN10,000 computer system. The major axis of the pattern are located and marked on the screen by the operator, then the computer determines the orientation of the crystal creating the pattern and stores the orientation information for later use.

Actual photos of these images were taken using electron imaging film placed inside the vacuum chamber. An example of one of these patterns is shown in fig. 14. To take this picture a film holder 30mm x 40mm was made to fit the end of the specimen exchange rod. The film is placed approximately 15mm from the sample and exposed for approximately 5 seconds. Exposure times varied with beam conditions, film distance from the sample and relative orientation on the vertical axis of the film with the specimen. Exposure times decreased with increases in beam intensity and/or decreases in film distance from the sample. The exposure intensity varied significantly along the vertical axis as the number and energy of the scattered electrons was a function of scattering angle. The electrons which strike the top of the film have undergone a larger degree of inelastic scattering then those that strike the lower portions of the film. There is a corresponding loss in electron energy and intensity at the upper portion of the film as the electrons

lose some energy every time they are inelastically scattered. The result is a large variation in electron intensity from the top to the bottom of a piece of film. Again a 20 kV accelerating voltage was used but the working distance was varied to change the relative vertical orientation between the film and specimen.

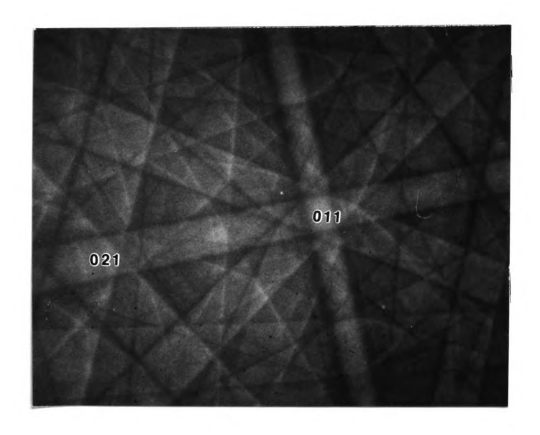


Figure 14. EBSP image generated from an FeAl sample using a 20kV accelerating voltage on a LaB<sub>k</sub> filament.

#### RESULTS

### Optical Microscopy

examined. There are several features which should be noticed about these figures. First, the powder processed materials have much smaller grain size than do the cast materials following extrusion, regardless of extrusion temperature or reduction ratio. Second, while there is a substantial increase in average grain size of the cast material after the 1000°C heat treatment there is only a modest gain in grain size after the same heat treatment for the powder processed material. Other general trends worth noting are the decrease in grain size with increased boron content and/or decreased extrusion temperature.

Figure 15 shows micrographs of the Fe-40at\*Al+0.1B powder processed material in the as-extruded state. These micrographs are representative of the microstructures found in the powder processed material after both single and double extrusion processing. The longitudinal view shown in fig. 15a shows small equiaxed grains with oxide stringers running parallel to the extrusion axis. The transverse view shown in fig. 15b also shows equiaxed grains, but now the stringers are seen end on and appear as rings of inclusions on the grain surfaces. It is apparent in both micrographs that the oxides did not prevent grain boundary migration

Table III. Grain sizes of the FeAl alloys before and after heat treatments [3].

## Grain Sizes

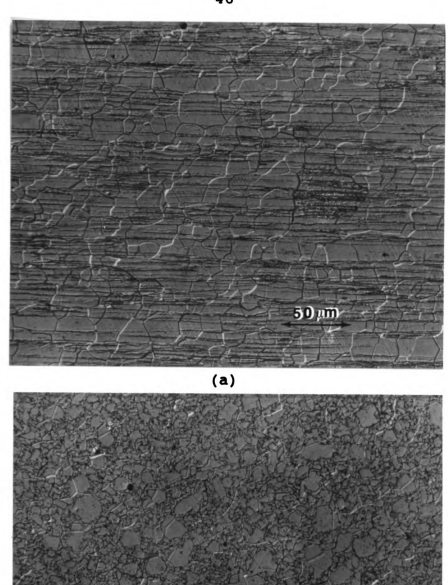
| Material  | As-Extruded           | 1000°C       | 1100°C           | 1200°C |  |  |  |  |  |
|---|-----------------------|--------------|------------------|--------|--|--|--|--|--|
| Single extruded 16:1 at 977°C from powder                   |                       |              |                  |        |  |  |  |  |  |
| Fe-40at%Al<br>Fe-40at%Al+0.1B                               | 18.7µ<br>14.8         | 28.7<br>25.9 | 27.0<br>25.5/231 | 240    |  |  |  |  |  |
| Double extruded 8:1 at 977°C then 6:1 at 800°C from powder  |                       |              |                  |        |  |  |  |  |  |
| Fe-40at%Al<br>Fe-50at%Al                                    | 10.3µ<br>11.0         |              |                  |        |  |  |  |  |  |
| Material  | As-Extruded           | 1000℃        | 1050℃            |        |  |  |  |  |  |
| Double extruded 8:1 at 977°C then 6:1 at 1077°C from powder |                       |              |                  |        |  |  |  |  |  |
| Fe-40at%Al<br>Fe-40at%Al+0.2B<br>Fe-50at%Al                 | 16.7µ<br>10.7<br>24.5 | 11.5         | 20.1/276         |        |  |  |  |  |  |
| Single extruded 16:1 from cast billets                      |                       |              |                  |        |  |  |  |  |  |

455 602

103μ 55

Fe-40attAl Fe-40attAl+0.1B

<sup>\* -</sup> Grain sizes of matrix grains vs abnormal grains.



(b)

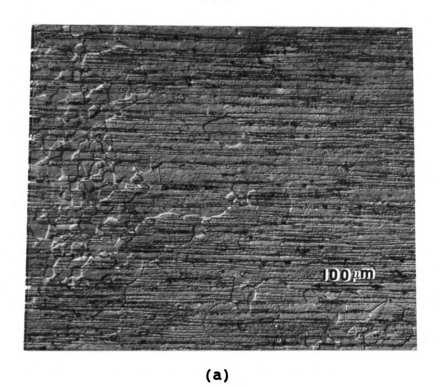
50 µm

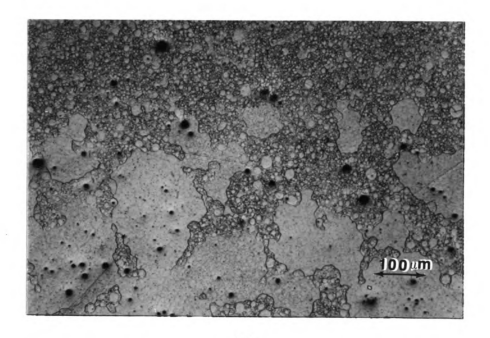
Figure 15. Micrographs of powder processed Fe-40at%Al+0.1B single extruded 16:1, (a) shows the longitudinal view [3] and (b) the transverse.

during recrystallization at these extrusion temperatures as there is no tendency for the grain boundaries to lie along the stringers.

Figure 16 shows micrographs of the single extruded Fe-40at%Al+0.1B material after 1100°C heat treatment. Two very different microstructures are evident in the micrographs. First there is the fine equiaxed grains of the original matrix and second, the large grains produced by abnormal grain growth. Figure 16a shows the longitudinal view of the material. The microstructure characteristics of the original matrix grains are basically unchanged from the asextruded condition. The grains which have grown in an abnormal manner, however, have become much larger then the matrix grains and tend to be oblong in the extrusion direction. Grains of this shape resulting from grain growth indicates a preference for growth along the extrusion axis. This theory is supported by fig. 16b showing the transverse view of the material where it appears the abnormal grains have grown up through the matrix.

Figure 17 shows micrographs of the single extruded Fe-40at%Al+0.1B after 1200°C heat treatment. The microstructure seen here is that of a material after normal grain growth. The grain size has increased substantially from the as-extruded state and the grains are all equiaxed with a rather narrow grain size distribution.





(b)

Figure 16. Micrographs of powder processed Fe-40at\*Al+0.1B single extruded 16:1 and heat treated 24 hrs. at 1100°C, (a) shows the longitudinal view [3] and (b) the transverse.

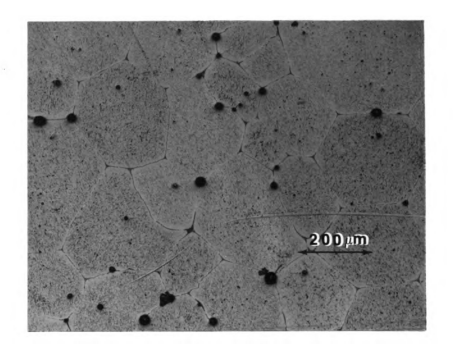


Figure 17. Micrograph of powder processed Fe-40at%Al+0.1B extruded 16:1 and heat treated 24 hrs. at 1200°C, transverse view.

The micrograph in fig. 18 shows a microstructure typical of the cast material in the as-extruded state. The two major differences between the cast and powder processed material are seen by comparing this micrograph to those in fig. 15. First, the average grain size of the cast material is significantly larger then that of the powder processed material and second the cast material is much cleaner. There is only a fraction of the oxides present in the cast material and this difference is important to note as it plays an important role in the behavior of the material.

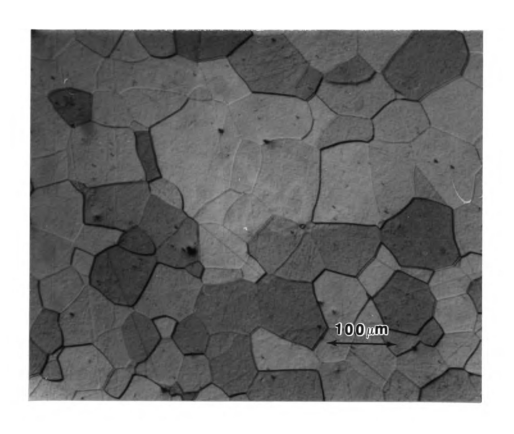


Figure 18. Micrograph of cast Fe-40at%Al+0.1B extruded 16:1 in the as-extruded state [3]. Longitudinal view.

### X-Ray Analysis

Shown in fig.12 was a diffraction pattern for the transverse direction of the single extruded Fe-40at%Al+0.1B powder processed material in the as-extruded state. This pattern is representative of the diffraction scans for all the powder processed material prior to significant grain growth. The first evidence of a significant texture in the material is seen in the diffraction data. Table IV compares the relative peak intensities seen here and those found in the published powder diffraction files. The intensity of the (111) peak in this material is several times larger then the published data while the (001) peak is not present at all. This indicates the presence of a preferred orientations in the material. Though there are methods of determining texture information from diffraction scans, the more rigorous pole figure goniometer method will be used in this study.

Table IV. Comparison of relative peak intensities between FeAl powder from published data and the extruded form.

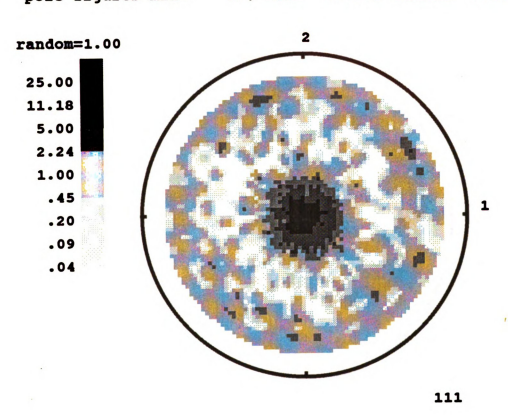
| Published Powder<br>Diffraction Data | <u>100</u> | <u>110</u> | <u>111</u> | <u>200</u> | <u>210</u> | 211 |
|--------------------------------------|------------|------------|------------|------------|------------|-----|
|                                      | 12         | 100        | 4          | 8          | 3          | 20  |
| Fe-40at%Al+0.1B                      | -          | 100        | 38         | _          | -          | 16  |

#### Powder Processed Material

Pole figures for transverse cross sections of single extruded Fe-40at%Al+0.1B powder processed material are shown in fig. 19. The material shown in this figure was extruded to an area reduction of 16:1 at 977°C. The pole figure for the {111} family of planes is shown in fig. 19(a). large symmetric peak in the center of the figure indicates a strong {111} wire texture in the material. Figure 19(b) and 19(c) show pole figures for the {110} and {211} families of planes respectively. The {110} pole figure shows the majority of the {110} planes lying approximately 35° from the extrusion axis in a symmetric ring. The {211} pole figure shows a similar ring approximately 20° from the extrusion axis. These later two pole figures give no evidence of secondary texture and confirm the {111} wire texture as the angle between the {111} and {110} planes is 35.3° and the angle between the {111} and {211} planes is 19.5°.

As mentioned in the procedure, all the x-ray diffraction data was gathered in the form of pole figures like those just discussed. Pole figures, while being easy to understand, are not complete pictures of a materials texture. Several pole figures are required [58] to produce a comprehensive picture of a material's texture which is why three were shown and discussed in the previous paragraph. A more concise and efficient was to display this information

pole figures min= 1.; max= 2669.; median= 342;



(a)

Figure 19. Pole figures generated from a powder processed FeAl alloy, (a) displays the {111} family of planes, (b) the {110} and (c) the {211}.

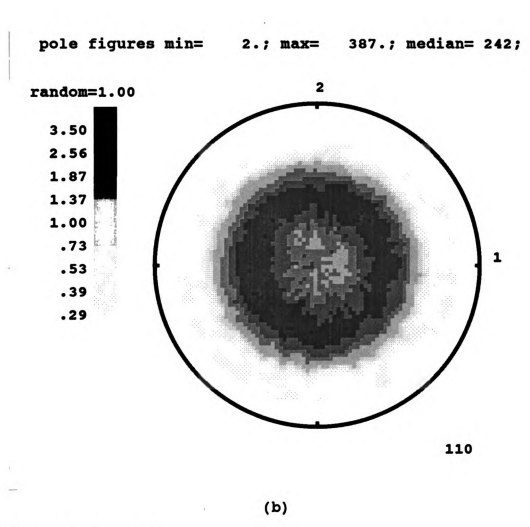


Figure 19. (cont.)

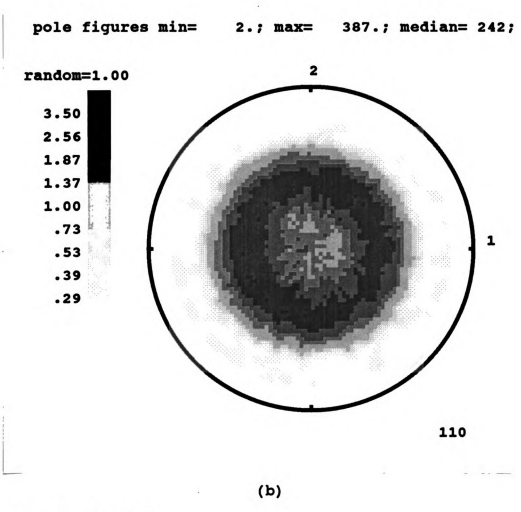
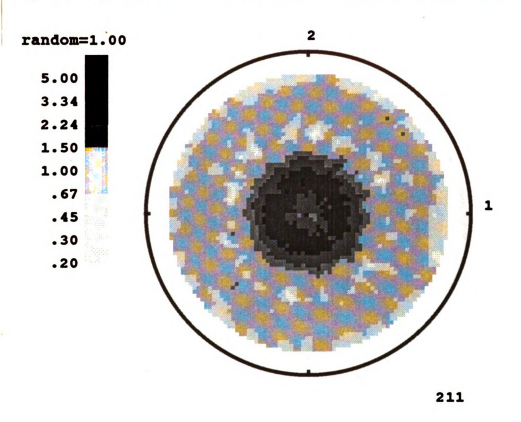


Figure 19. (cont.)

Figure





(c)

Figure 19. (cont.)

is in th

Inv

crystal a stere pole fi discuss densiti triangl to see way to in plac All of textur

> shown mater Wire off

transv

the ma

treat

grad Very

tre

hea

in

sa.

is in the form of inverse pole figures.

Inverse pole figures relate the relative density of crystallographic planes lying normal to a samples surface on a stereographic triangle. Figure 20(a) shows the inverse pole figure generated from three pole figures like those discussed above. In this figure we see a peak in the pole densities in the <111> direction on the stereographic triangle indicating a <111> texture component. It is easy to see that the inverse pole figures are a more efficient way to display texture information, thus they shall be used in place of pole figures for the remainder of this study. All of the material examined in this study possessed a wire texture so only a single inverse pole figure of the transverse orientation is needed to describe the texture of the material in question.

Inverse pole figures from before and after heat treatments of the Fe-40at%Al material extruded 16:1 are shown in fig. 20. Figure 20(a) shows the texture of the material in the as-extruded state to have a strong <111> wire texture component. The intensity of the texture falls off rapidly to below random in the <001> direction and gradually to just a few times random in the <011> direction. Very little change in the texture occurred during heat treatment at 1000°C as shown in fig. 20(b). The material heat treated at 1100°C displayed two very different textures in the same sample. Figure 20(c) shows one side of one sample displaying a dominant <111> wire texture similar to

7

Fig

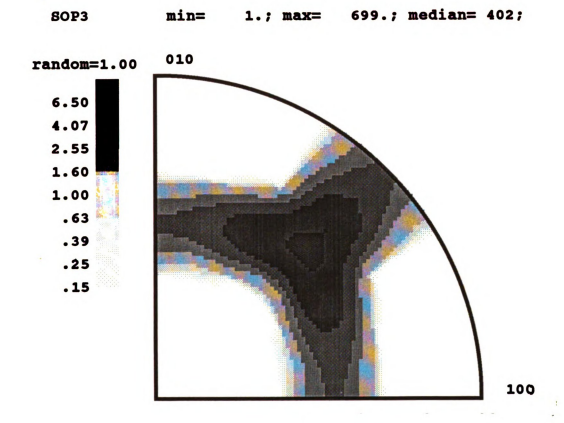


Figure 20. Inverse pole figures for the powder processed Fe-40at\*Al material extruded 16:1, (a) displays the texture prior to heat treatment, (b) the 1000°C, (c) the 1100°C none grain growth, (d) the 1100°C with bimodal grain growth.

(a)

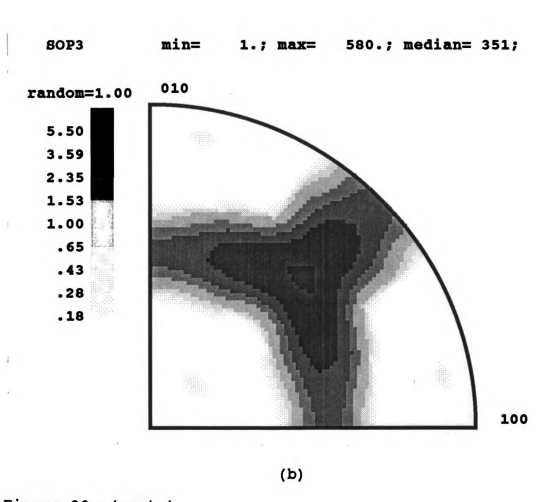


Figure 20. (cont.)

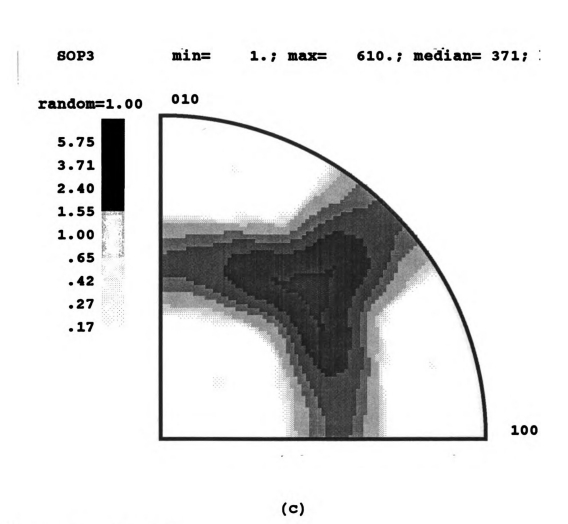


Figure 20. (cont.)

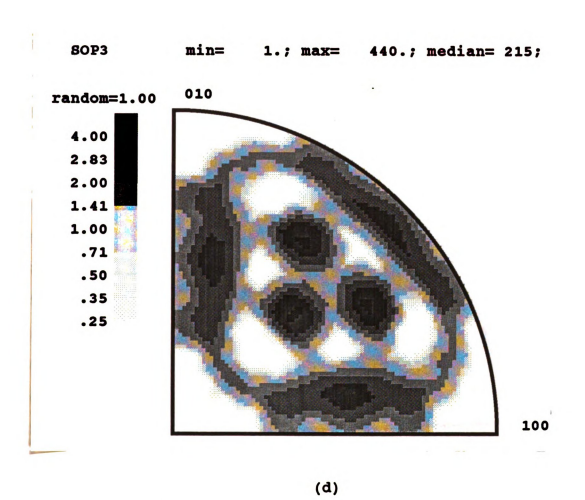


Figure 20. (cont.)

that observed in the as-extruded and 1000°C material. The opposite side of the same sample displayes a different texture indicating a change in the microstructure which, as will be shown later, is a result of bimodal grain growth. This texture is much weaker and is has two peaks, one centered about the <211> direction and another slightly weaker peak about the <441> directions.

Inverse pole figures for the single extruded powder processed Fe-40at%Al+0.1B material are shown in fig. 21. Figure 21(a), the as-extruded material, shows a texture very similar to that shown in Fig. 20(a) for the Fe-40at%Al in the as-extruded condition. A slight sharpening of the texture occurred during heat treatment at 1000°C as shown in fig. 21(b). After heat treatment at 1100°C again two very different textures were found in the material. One sample displayed a <111> texture very similar to that found in the sample heat treated at 1000°C seen in fig. 21(c). A different surface from the same sample, however, shows a very different texture as seen in fig. 21(d). The texture here is weaker and has shifted from the <111> direction of the original extruded material to a band of running from the <114> to the <103> directions. Like the Fe-40at%Al discussed above this drastic shift in preferred orientation indicates a major change in microstructure which is the result of bimodal grain growth. Unlike the material previously discussed, the shift in texture appears to be an organized shift to a new preferred orientation. Further

e١

r

p

s

t

evidence of this will be seen in the EBSP section of the results. The inverse pole figure for the single extruded powder processed material after heat treatment at 1200°C shown in fig.21(e). This material displays a fairly general texture with components from the <111> direction to the <110>, with a minor peak about the <221> direction. The microstructure shows no evidence of bimodal grain growth and the texture supports this as there is general dissipation of the as-extruded texture in the <110> direction as opposed to a discontinuous shift from one orientation to another.

Inverse pole figures for double extruded powder processed Fe-40at\*Al+0.2B material are shown in fig. 22. Again the as-extruded and 1000°C material show a predominantly <111> wire texture (fig. 22(a) and 22(b)). The material heat treated at 1050°C is shown in fig. 22(c) and again there has been a major change in the texture due to abnormal grain growth. However, unlike the 1100°C single extrusion sample this shift in texture is fairly well centered around the <103> direction. It should be noted the large grain sizes produced by abnormal grain growth, in both the single and double extruded material, results in marginal statistics for x-ray analysis.

To examine the effect of double extrusion and extrusion temperature on texture material was examined after a single extrusion with 8:1 reduction ratio then re-extruded with area reduction of 6:1 at two different temperatures. The inverse pole figure for Fe-40at%Al powder single extruded to

8

rar

Fig

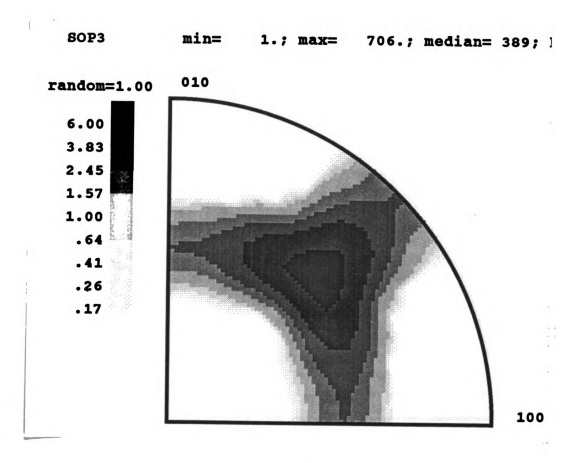


Figure 21. Inverse pole figures for the powder processed Fe-40at&A+0.1B material extruded 16:1, (a) displays the texture prior to heat treatment, (b) after 1000°C, (c) after 1100°C with no little grain growth, (d) after 1100°C with bimodal grain growth and (e) after 1200°C.

(a)

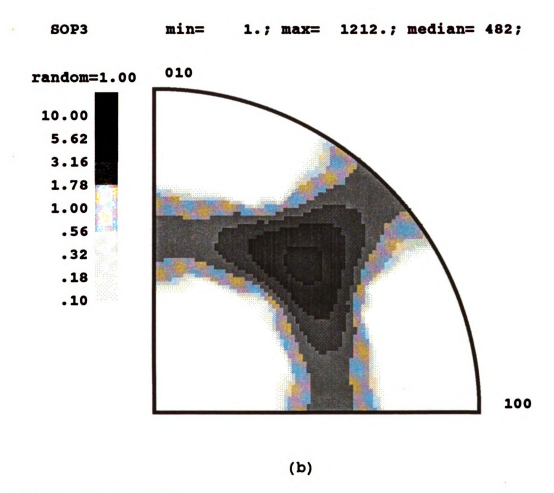


Figure 21. (cont.)

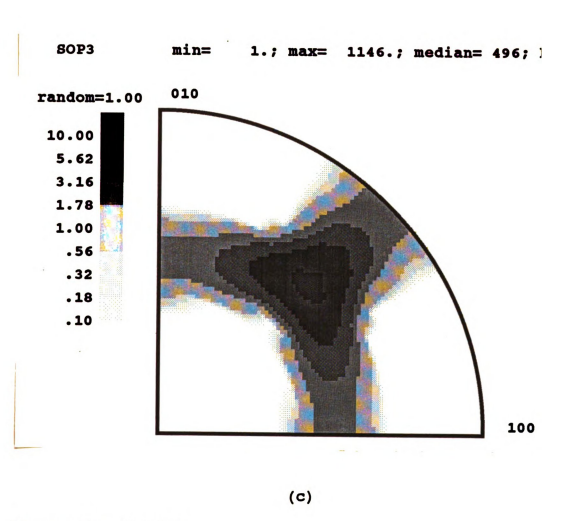
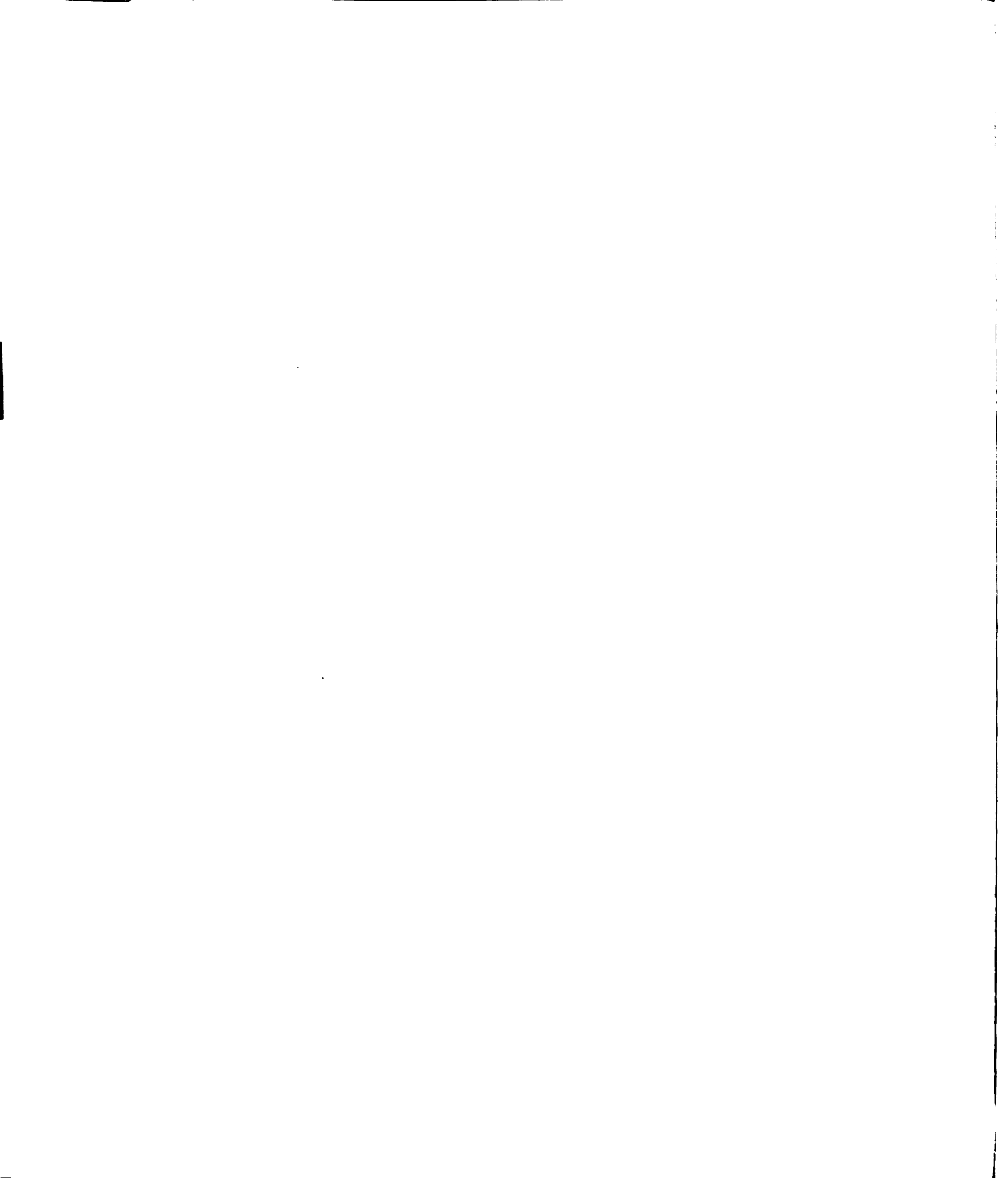
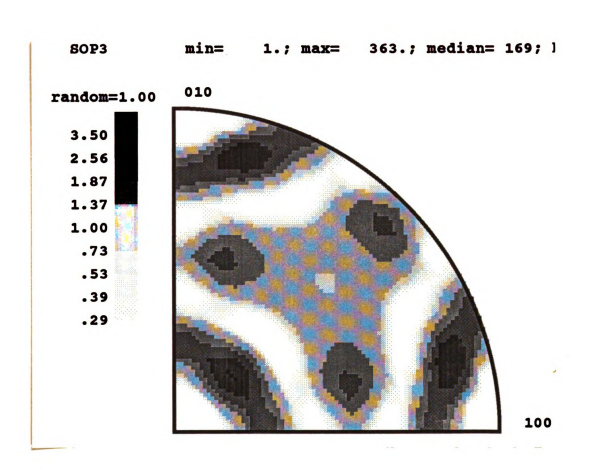


Figure 21. (cont.)





(d)

Figure 21. (cont.)

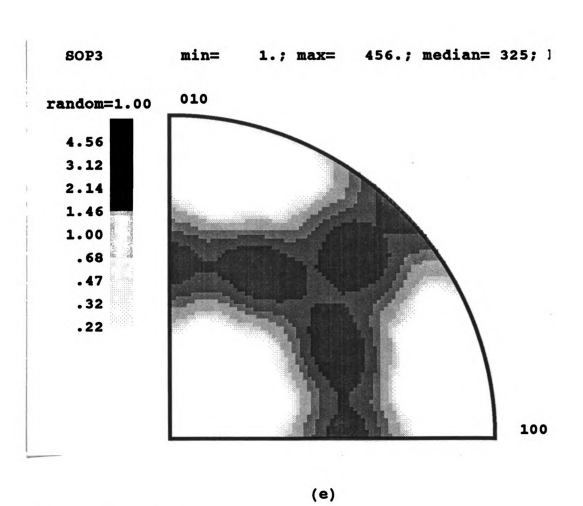


Figure 21. (cont.)

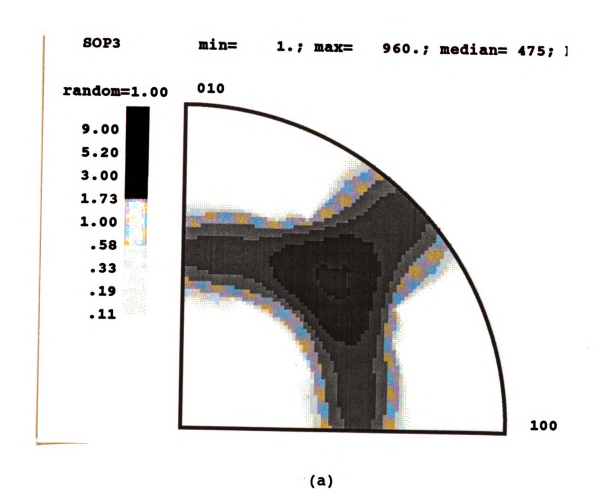


Figure 22. Inverse pole figures of the powder processed Fe-40at\*Al+0.2B material double extruded, (a) displays the texture prior to heat treatment, (b) after 1000°C and (c) after 1050°C.

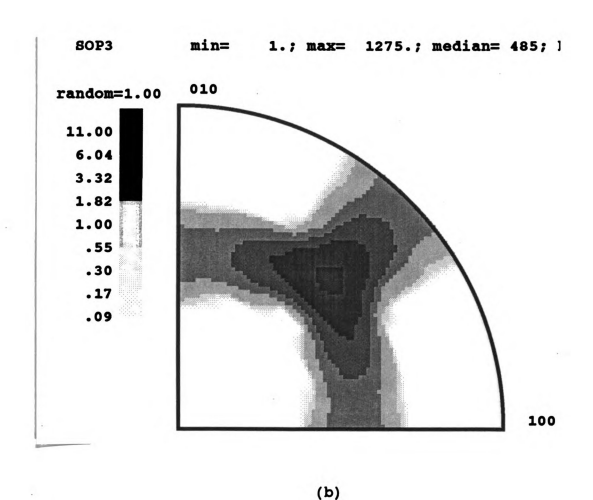


Figure 22. (cont.)

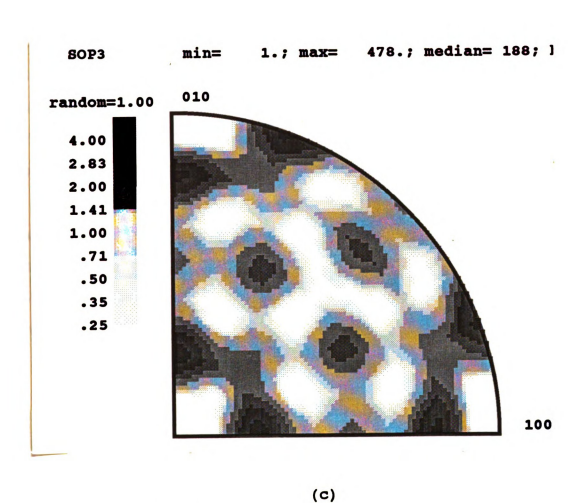


Figure 22. (cont.)

an 8:1 reduction ratio is shown in fig. 23(a). This material also shows the <111> wire texture but the texture is not as sharp as that extruded 16:1. This same material was then extruded a second time at two different extrusion temperatures. The inverse pole figures for these are shown in fig. 23(b) and 23(c). A second extrusion at 800°C with an area reduction of 6:1 had little effect on the texture, while re-extrusion at 1075°C with 6:1 reduction caused a considerable sharpening of the <111> texture component.

Figure 24 shows inverse pole figures of the Fe-50at%Al material after a double extrusion processing the same as discussed above. The results are almost identical to those of the double extruded Fe-40at%Al. Again the material which received a second extrusion at 800°C (fig. 24(a)) showed little change in texture while a second extrusion at 1075°C (fig. 24(b)) showed the sharpest texture seen in this study.

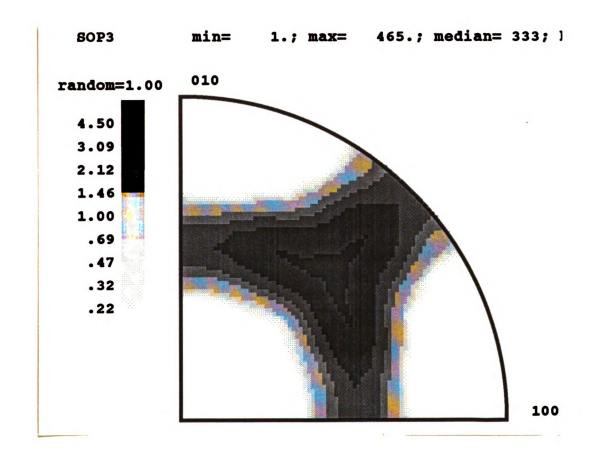
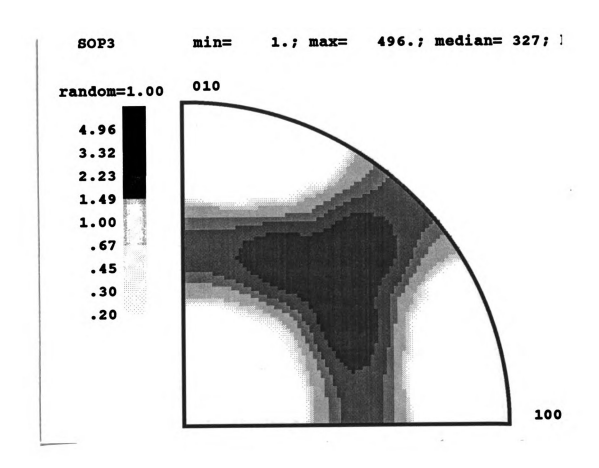


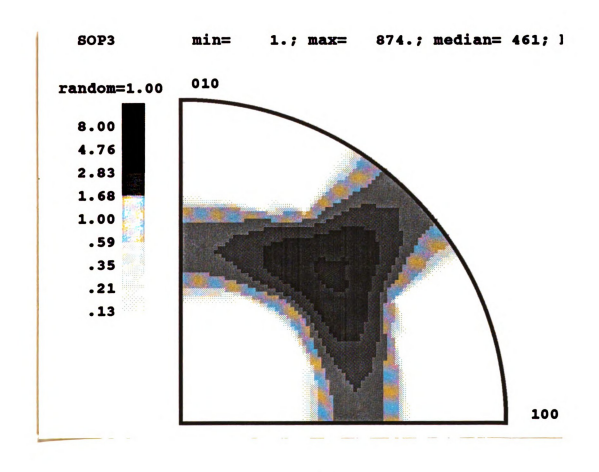
Figure 23. Inverse pole figures of powder processed Fe-40at\*Al single and double extruded, (a) single extruded 8:1 at 977°C, (b) after a second 6:1 extrusion at 800°C and (c) after a second 6:1 extrusion at 107°C.

(a)



(b)

Figure 23 (cont.)



(c)

Figure 23. (cont.)

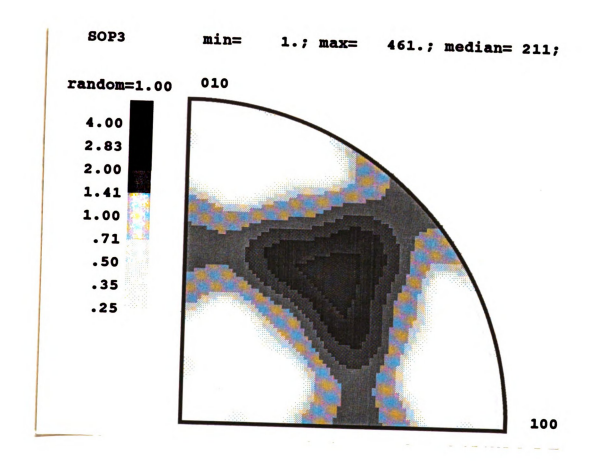
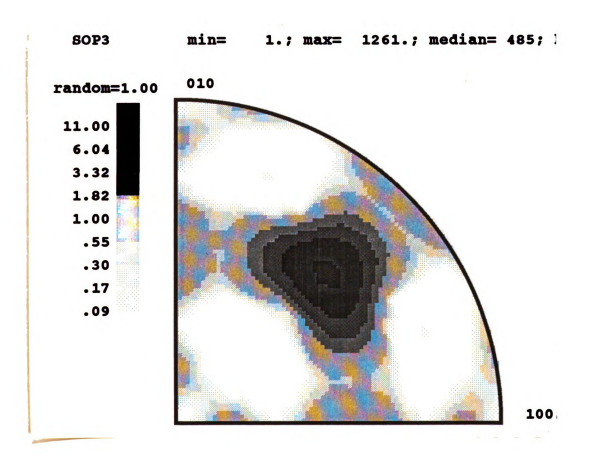


Figure 24.

Inverse pole figures of double extruded Fe-50at%Al receiving the second extrusion at different temperatures, (a) second extrusion at 800°C and (b) at 1077°C.

(a)



(b)

Figure 24. (cont.)

## Cast Material

The x-ray results for the cast and extruded material without boron are shown in fig. 25. These results are very similar to the those found in the powder processed material. As shown in fig. 25 the texture has the same strong <111> component.

Figure 26 shows an inverse pole figure for the cast and extruded material with boron. This material does not show the strong <111> texture seen in the as-extruded state exhibited by the powder processed material. Instead, the strongest component is in the <110> direction with a weaker <111> component. Heat treatment of the cast material resulted in a very large grain size and as a consequence was statistically unsuitable for x-ray analysis.

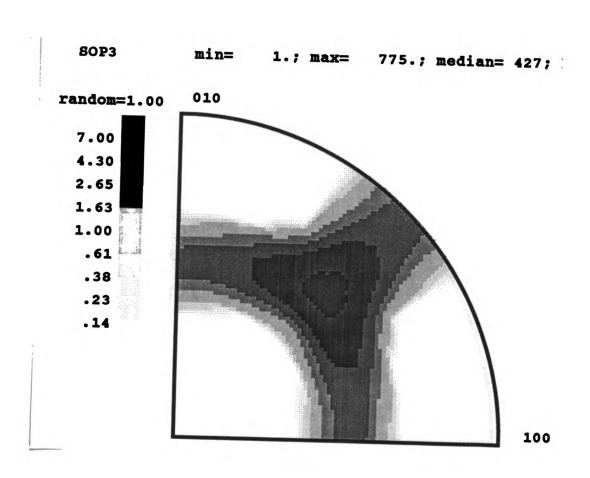


Figure 25. Inverse pole figure of the Fe-40at%Al cast and extruded material.

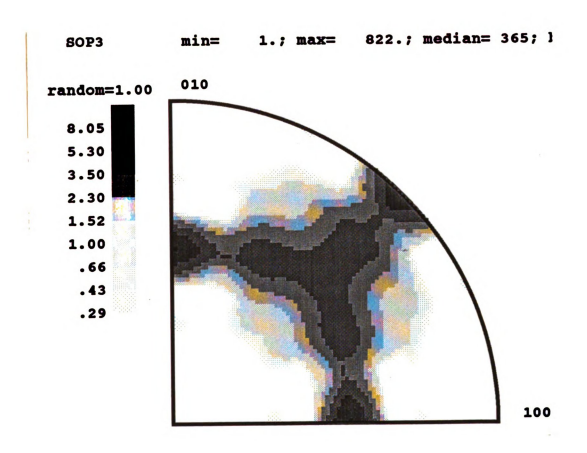


Figure 26. Inverse pole figure of Fe-40at%Al+0.1B cast and extruded material.

## EBSP Results

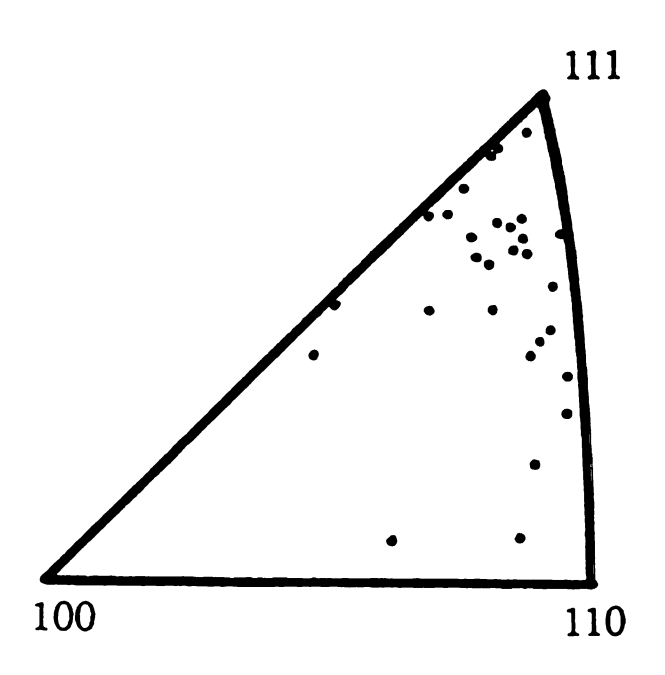
The results from the EBSP experiments are presented as inverse texture plots where each point represents the orientation of an individual grain. All of the texture plots shown in this study will be of the transverse direction of the sample so the direction in the grain which is parallel to the extrusion axis will be represented on the plot ( i.e. a point on the (111) pole indicates the <111> direction of the grain in question is parallel to the extrusion axis). The advantage of EBSP is its ability to determine the orientation of individual grains on the microscopic level [59,60]. EBSP was used in two ways in this study. First, it was used to support the texture analysis done with x-ray diffraction by producing pole and inverse pole figures from randomly selected grains. Second, and more importantly, it was used on specimens which displayed bimodal grain growth to examine grains that grew in a normal fashion separately from those which grew in an abnormal way.

The inverse texture plot for the 16:1 single extruded Fe-40at%Al are shown in fig. 27. The inverse texture plot shown in fig. 27(a) was generated by taking orientations from randomly selected grains to create a plot which will be representative of the material. The cluster of grain orientations near the <111> direction on the unit triangle confirms the results of the x-ray analysis which indicated a <111> wire texture. Figure 27(b) shows the plot for the Fe-

40at Al material after heat treatment at 1000°C. Again the plot confirms the <111> texture found during x-ray analysis. The examination of the material heat treated at 1100°C is shown in fig. 27(c) and 27(d). As in the x-ray analysis two different textures were found very near each other in the same sample. The EBSP results shown in fig. 27(c) show the <111> texture seen in fig. 20(c) of the x-ray analysis. Figure 27(d) shows the results from the other side of the sample. The x-ray analysis of this surface (fig 20(d)) appeared to indicate a weak <211>, <441> texture.

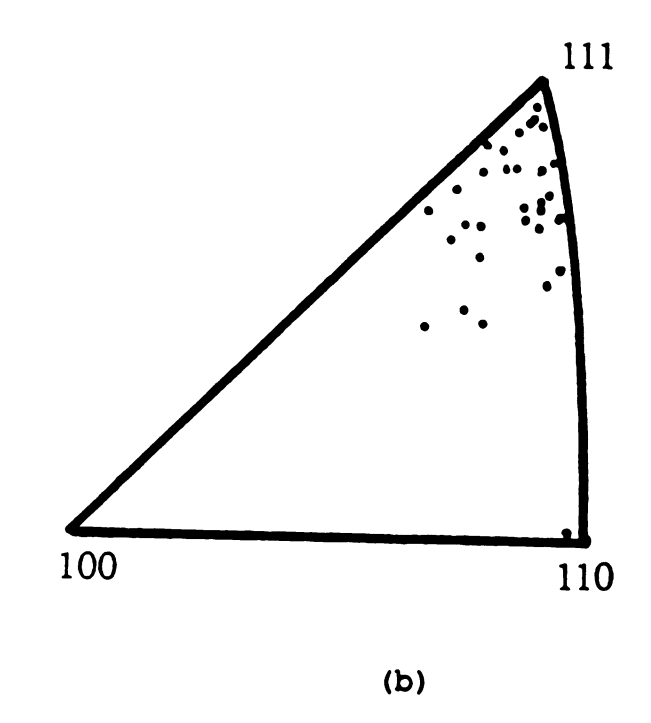
Figure 28 shows the inverse texture plots for the single extruded Fe-40at%Al+0.1B material. Again the plots for the as-extruded and 1000°C material support the x-ray analysis and confirm the <111> texture of the material.

Figures 28 (c) and 28 (d) show the EBSP results for the material heat treated at 1100°C. On this surface the EBSP was used to examine the orientations of the growing grains separately from the stagnant grains of the original matrix. Grain orientations taken from the areas on the sample which have not yet been consumed by abnormal grain growth are seen in fig. 28 (c). These grains are all small (15-25 microns) and show the <111> texture of the original matrix. Reviewing the inverse pole figure generated from the x-ray analysis (fig 21 (d)), little evidence of these <111> oriented grain is seen. This is due to extensive bimodal grain growth dominating the surface area on the sample



(a)

Figure 27. Inverse texture plots for the 16:1 single extruded Fe-40at\*Al material, (a) shows orientations from grains prior to heat treatment, (b) after 1000°C, (c) after 1100°C with little grain growth and (d) after 1100°C with bimodal grain growth.



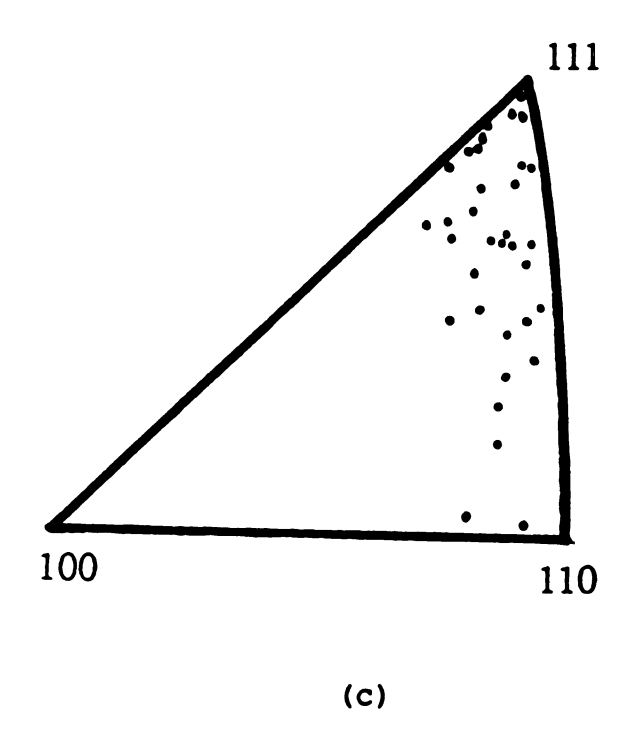
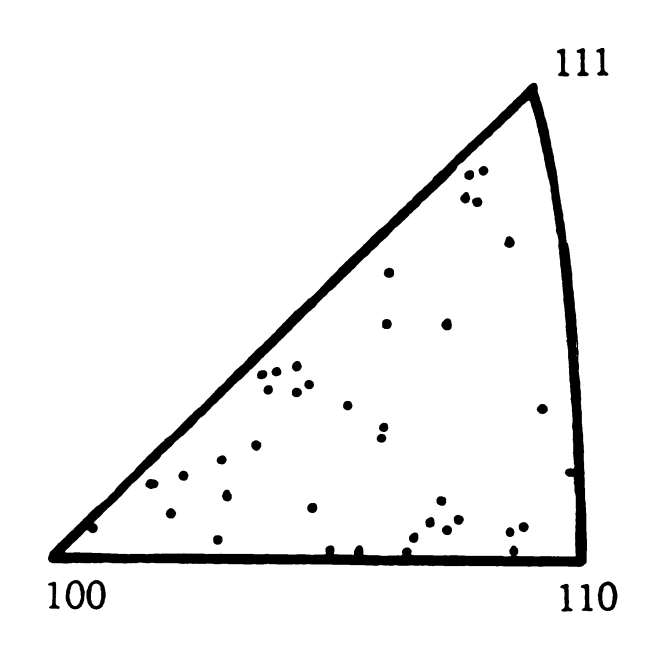


Figure 27. (cont.)



(d)

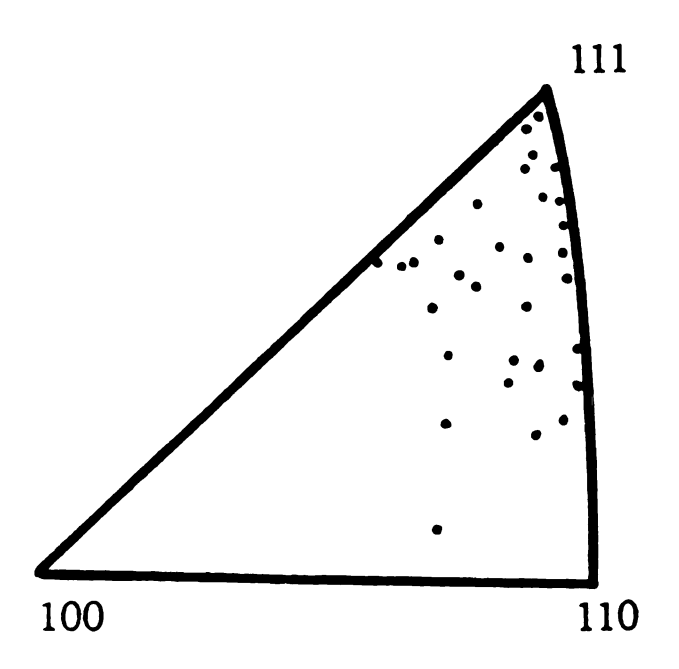
Figure 27. (cont.)

leaving only a small fraction of the surface area having the <111> texture of the original matrix. Grain orientations taken from the areas of abnormal grain growth are seen in fig 28 (d). This plot shows a dramatic, fairly well organized, shift in orientation away from the <111> direction. These grains are all much larger (50-300 microns) and have orientations forming a band from the <114> to the <103> directions similar to that seen in the x-ray analysis.

The inverse texture plot for the Fe-40at%Al+0.1B material heat treated at 1200°C is shown in fig. 28(e). The micrograph of this material shown in fig. 17 shows a stabilized microstructure of equiaxed grains. The EBSP analysis shows a good deal of scatter about the <111> texture of the original matrix grains. As discussed above this is due to the dissipation of the as-extruded texture by normal grain growth.

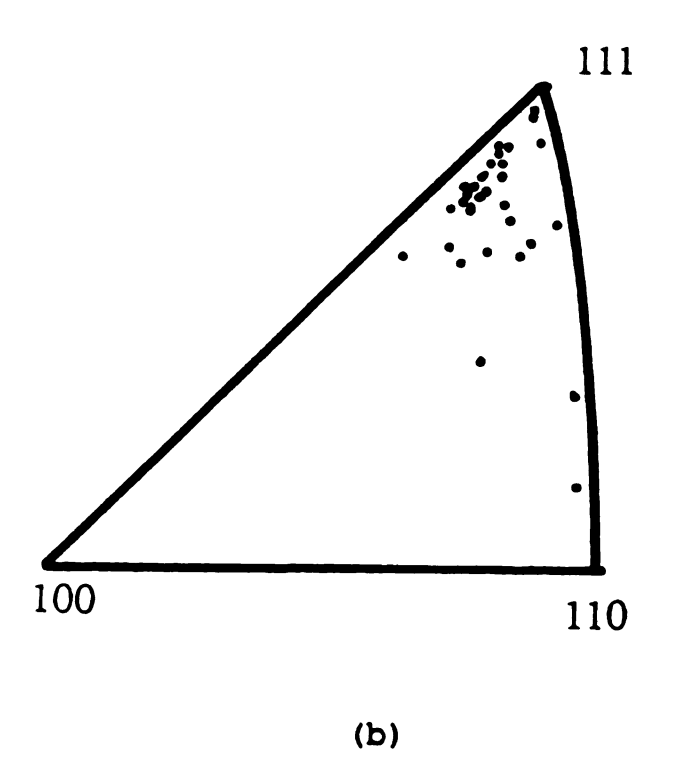
Figure 29 shows EBSP results from the double extruded Fe-40at%Al+0.2B material. Again the inverse texture plots from the as-extruded and 1000°C material show the <111> texture confirming the x-ray results.

The EBSP analysis of the 1050°C material was separated into two groups, as before, due to the presence of abnormal grain growth. Grain orientations taken from areas on the sample that have not yet been consumed by abnormal growth are displayed in fig. 29. Similar to the single extruded 1100°C material, these grains were all relatively small



(a)

Figure 28. Inverse texture plots of the 16:1 single extruded Fe-40at%Al+0.1B material. (a) shows orientations from grains prior to heat treatment, (b) after 1000°C, (c) after 1100°C from original matrix grains, (d) after 1100°C from abnormal grains only and (e) after 1200°C.



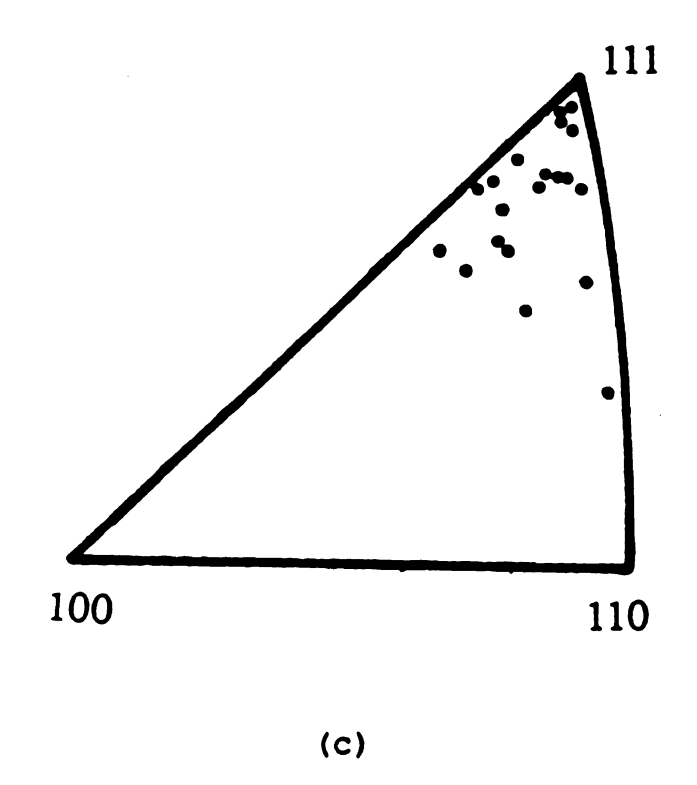
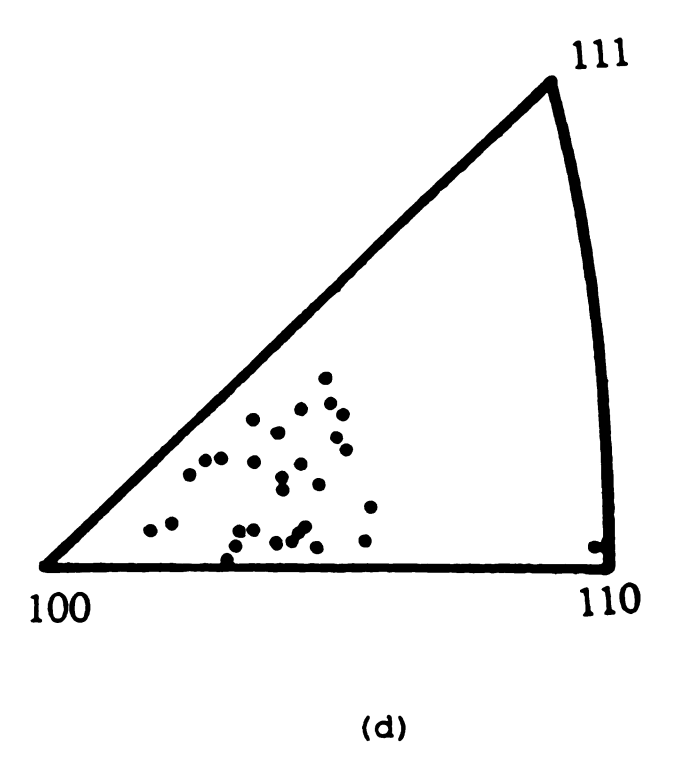
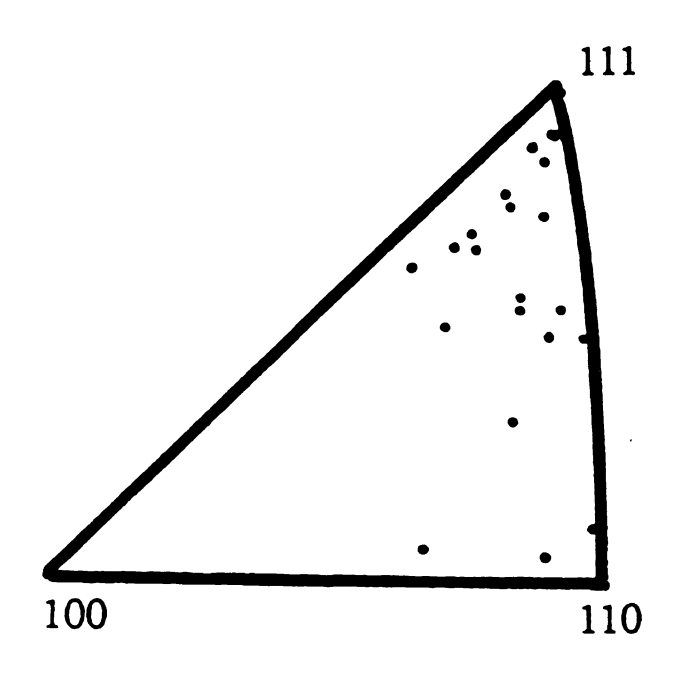


Fig. 28. Cont.

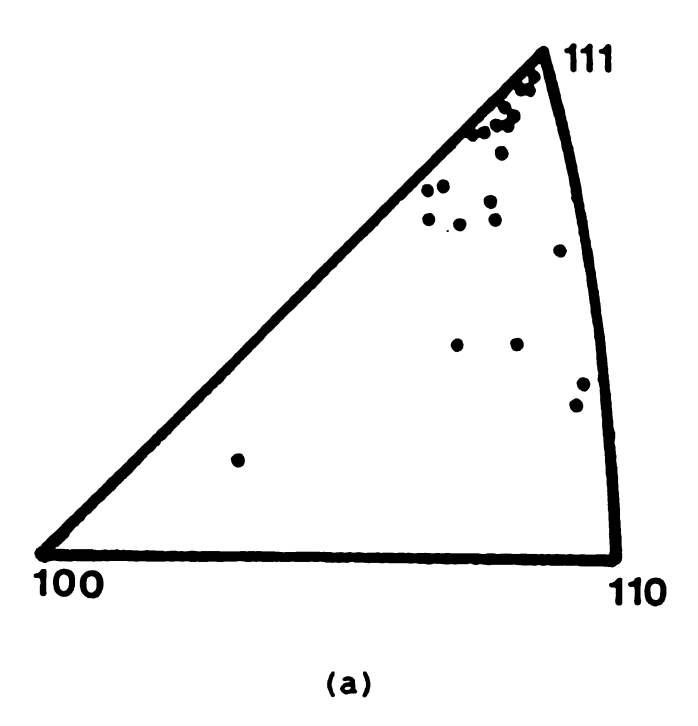




(e)

Fig. 28. Cont.

(15-25 microns) and display the <111> orientation of the original matrix. The plot showing the orientations of the grains which grow in an abnormal fashion are shown in fig. 29. These grains varied significantly in size (50-400 microns) and possessed orientations approximately 40° away from the <111>, centering on the <103> direction.



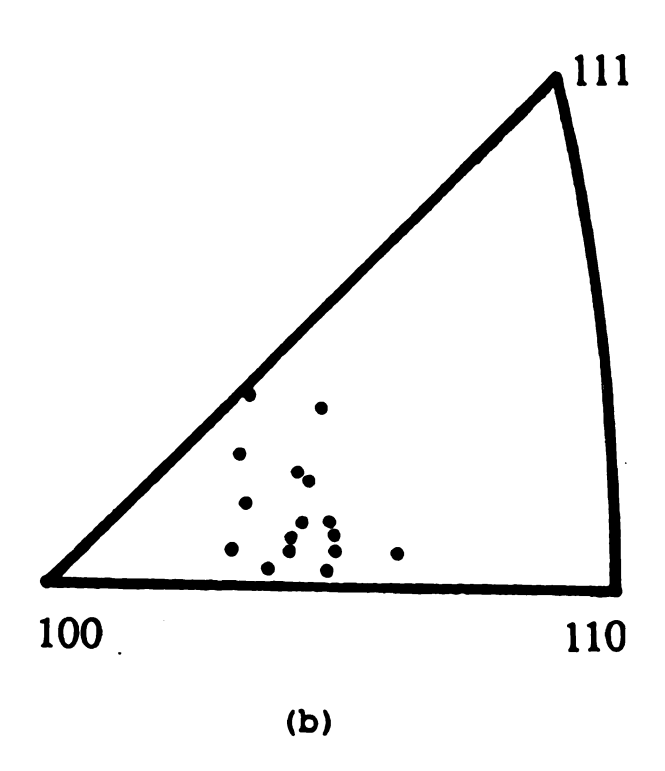


Figure 29. Inverse texture plot for the double extruded Fe-40at%Al+0.2B material. (a) shows orientation from grains after 1050°C heat treatment from original matrix grains only and (b) after 1050°C heat treatment from abnormal grains only.

## Cast Material

As stated in the x-ray section of these results the grain size of the cast material after heat treatment is too large for good x-ray analysis, thus the only texture information presented is from EBSP. The inverse texture plot for cast material with boron heat treated at 1050°C are shown in fig. 30. While the as-extruded cast material displays a <110> texture, the material heat treated at 1050°C shows fairly random distribution of orientations.

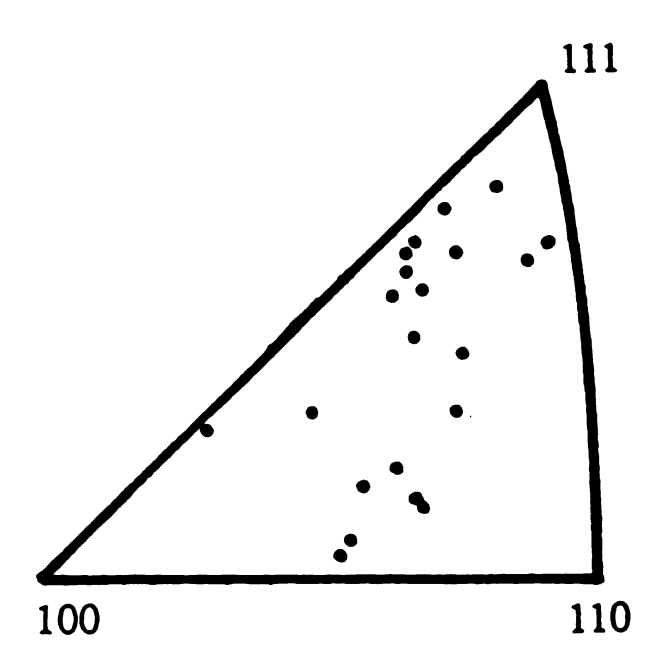


Figure 30. Inverse texture plot of cast and extruded Fe-40at%Al+0.1B.

## DISCUSSION

In the previous section the results from optical, x-ray and EBSP examinations were presented. These results will now be analyzed in an effort to better understand the microstructure and texture evolution of this material.

A strong contrast is evident in the results between the powder processed material and the cast material. This is due to a large difference in the initial condition of these materials, meaning whether it is produced by hot extrusion of a powder or a cast billet. Evidence of this is seen by comparing the grain sizes of the two materials in the asextruded state (table 2). The materials are similar in composition and are extruded under similar conditions yet, there is a significant difference in the resulting grain size. The powder processed materials, regardless of single of double extrusion processing, exhibits relatively small grain sizes ( 10-25 microns ) in the as-extruded state while the cast and extruded materials display much larger grain sizes (50-100 microns). There is also a significant difference in impurity content of the two types of materials which, as will be discussed later, plays a major role in the evolution of the microstructures. For these reasons the cast and powder processed material will be discussed separately.

## Powder Processed Material

## The As-Extruded State

#### Microstructure

The condition of the material in the as-extruded state is very similar for all of the powder processed material. The grain sizes are small, from 10 to 25 microns, and they all possess a strong <111> wire texture. The small initial grain size is a result of processing and shows some variation with changes in processing conditions and material composition. The size of initial powder particles varied from approximately 2 to 30 microns in diameter. When hot extruded, the oxide surfaces of the particles break up to produce stringers of oxide inclusions running parallel to the extrusion axis as seen in the results section. The initial microstructures display small equiaxed grains with the oxide stringers running throughout the matrix. This indicates the materials have recrystallized during hot extrusion.

It is apparent that the oxide stringers have had only a limited influence on the recrystallization process. The equiaxed microstructure with stringers running randomly through the grains indicates that the oxides did not prohibit grain boundary migration during recrystallization of the strained matrix. This may appear to contradict the obvious pinning effect the oxides have during heat treatment at similar temperatures but upon closer examination it does

not. Even though the temperatures of the heat treatments were the same or higher, the driving forces behind the grain growth is different. During hot extrusion the grains are deformed, resulting in significant amounts of stored energy in the lattice. This energy is released during recrystallization providing much of the driving force for recrystallization. During the subsequent heat treatments this energy source is not present, having already been released. The driving forces for boundary migration during recrystallization are, in general, much larger than the pinning forces exerted by particles in a matrix [61]. Calculations by Hazzledine [61], using generalized values, show the driving forces for recrystallization to be several orders of magnitude larger then the Zener pinning forces exerted by particles. In contrast, the driving force for migration in an unstrained matrix is on the same order of magnitude as that of the pinning forces. This implies that while recrystallization may be slowed by the presence of the oxides, it is not severely restricted. Once recrystallization is complete, however, any further grain growth will be very sluggish. It is likely that this is what is happening during the hot extrusion of this material.

The primary factors controlling the recrystallized grain size are the material grain size prior to extrusion [46,62], extrusion temperature [46,62,63], composition [46,64] and inclusion content [61,65-67]. The extent of their influence depends on the extrusion conditions. For

example, it is generally excepted that the grain size prior to extrusion is the major factor influencing the post extrusion grain size [46,48,62]. This is due to the tendency of new grains to nucleate at pre-existing grain boundaries. This is the reason for the large differences in grain sizes between the powder processed and the cast materials of this study, as in a previous study [3] it was noted that prior to extrusion the cast material had average grain sizes on the order of several hundred microns. Yet very large variations in grain size can also be achieved with changes in any one of the controlling factors.

## Extrusion Temperature and Grain Size

The effect extrusion temperature has on grain size can be seen by comparing the grain sizes in the as-extruded condition of the double extruded Fe-40at%Al material, where the second extrusions were done at different temperatures. First the material was extruded from a powder at 977°C with a reduction ratio of 8:1 and allowed to cool. This material was spit into two groups with one group receiving a second extrusion at 800°C and the other at 1077°C. A 6:1 reduction ratio was used for both second extrusions. The material with the high temperature second extrusion had an average grain size approximately 60% larger than the low temperature material. Similar results are seen on examining the Fe-50at%Al material given the same processing. These variations in grain size with extrusion temperature are due

to the increase in boundary migration rate with increased temperature. As the extrusion temperature increases the rate of boundary migration for the recrystallized grains increases faster than the rate for nucleation of new grains [46,62]. This results in fewer new grains being nucleated as the recrystallized grains grow quickly eliminating the strained matrix and with it the area for new crystal nucleation sites. Thus fewer new grains are nucleated and the average grain size increases. Or conversely, lower extrusion temperatures allow more time for nucleation of new crystals in the strained matrix where grain growth is slow.

# Composition

There is also some variation in the grain size with boron content. The material with the highest boron content having the smallest grain size and the lowest boron content the largest grain size, regardless of single or double extrusion processing. It is well established that boron in this material segregates to the grain boundaries [5]. This acts to slow grain boundary migration during recrystallization [35,46,64,] resulting in smaller grain sizes.

## Texture

The powder processed material has a strong <111> wire texture after hot extrusion. This texture is developed

during the hot extrusion process. Whether this is a result of dynamic recrystallization while the material is still being deformed or post extrusion recrystallization as the material cools is unclear.

If the texture is developed by a dynamic recrystallization process it should be of the same orientation as the deformation texture [46,48,68]. This is a results of the deformation process continuing to rotate the grains, even as they are recrystallizing, to the orientation most favorable for the active slip systems in the material. If the texture is a result of continued recrystallization after deformation is finished it will be controlled by growth processes and may be completely different from the deformation texture of the material. Determining which of these mechanisms is acting in the materials being examined in this study is beyond the scope of this work and shall not be debated here.

The development of a texture by recrystallization following hot deformation may be explained with the following argument. Local variations in the density of dislocations arise during the deformation process. This is to some degree orientation dependent [69]. The number and size of subgrains formed at grain boundaries will vary correspondingly with the density of dislocations. This leads to the development of nuclei in parent grains with the most favorable orientations [70,71]. This will result in a preferred orientation for the formation of nuclei. The

nuclei will have orientations similar to the original parent grain and if the grain on the other side of the grain boundary has a different orientation, a large angle grain boundary will be present to help initiate grain growth [47]. This mechanism results in the elimination of grains with orientations poorly aligned for the processes needed for the development of nuclei. Grains which do develop with misaligned orientations will be likely be near grains with a more favorable orientations and be re-consumed by growing grains.

## The Effect of Temperature On Texture

There was no significant difference in the degree of texture between before and after a second extrusions at 800°C. The initial extrusions of the powders at 977°C developed moderate textures which were not noticeably changed during the second extrusions at 800°C. This implies a steady state condition has been reached for extrusion in this temperature range. If it is assumed that the powder consolidates early in the first extrusion, then once consolidated, the extrusion conditions will be similar and therefore produce similar driving forces to control the recrystallization.

A significant difference in the degree of texturing is observed in materials which received their second extrusion at 1077°C. These materials developed a tighter <111> wire texture then those extruded at 800°C. This, like the

increase in grain size, is a result of increased rates of grain growth at higher temperatures. At these temperatures grains with the <111> orientation in this material appear to have a grain growth advantage during recrystallization.

Preferred growth is not a new phenomenon and has been observed by other researchers [72,73]. Increasing the temperature has increased this advantage resulting in a larger volume of the matrix having the <111> orientation giving a sharper texture. Similar results have been reported by Bieler et.al. [73] working with powder processed NiAl.

## After 1000°C Heat Treatment

## Microstructure

The powder processed materials, regardless of composition and extrusion conditions, do not exhibit significant grain growth during heat treatment at 1000°C. This is mainly a result of the numerous oxide stringers present in the material. As discussed earlier these inclusions produce a drag force on the grain boundaries as they attempt to migrate past the particles [61,65]. Little can be said about the effect boron has on the grain growth behavior at this temperature since no significant difference is seen between material with or without boron. The dramatic influence the oxide inclusions have on the material overshadows any effect of the boron may produce. We can conclude, however, that the stagnant growth behavior is a

result of the inclusions since both the materials with and without boron behaved in a similar manner.

#### Texture

The sluggish grain growth during the 1000°C heat treatment results in a correspondingly small changes in the texture. What change there is is a slight sharpening of the original <111> wire texture in the case of the material containing boron. This tightening of the texture is further evidence of preferred growth in this material. If there was normal grain growth the wire texture of the material would tend to dissipate as grains with orientations away from the <111> wire texture would have high angle grain boundaries on all sides and therefore an advantage during grain growth.

It should be noted that while no abnormal grain growth was seen in this study in material heat treated at  $1000^{\circ}$ C, a previous work did observe abnormal growth in Fe-50at%Al after  $1000^{\circ}$ C heat treatment [3]. The reason for this may be that the melting temperature of Fe-50at%Al is lower than that of Fe-40at%Al resulting in a higher  $T/T_m$  for the Fe-50at%Al material.

## After 1050/1100°C heat treatment

## Microstructure

Significant bimodal grain growth occurs in the powder processed materials during the heat treatments of 1050°C and 1100°C. The result is a microstructure with two very

different grain types. Portions of the material still display the fine grained equiaxed microstructure of the asextruded matrix while other areas have developed very large elongated grains. The fine equiaxed grains have grain sizes only slightly larger then the grains in the as-extruded material indicating that the grain boundaries are still being effectively pinned. The larger grains in the matrix are several times as large as the fine equiaxed grains indicating they have been able to overcome the pinning forces of the oxides and are free to migrate. This type of microstructure was not present in the as-extruded material so it must have evolved during the 1050°C and 1100°C heat treatments as a result of bimodal grain growth.

## Microstructure and Texture

As discussed in the introduction, the two commonly excepted reasons for bimodal grain growth are the introduction of an unusually large grain into a matrix or the presence of a strong texture. The production of this material by the hot extrusion of a relatively fine powder leaves little chance for the development of abnormally large grains during production. There is no evidence to suggest something unusual is producing abnormally large grains during extrusion so it will be assumed that none exist in the matrix prior to heat treatment. This rules out the first theory on how abnormal grain growth is initiated.

The material is highly textured but only in one

dimension, not all three. Unlike a rolling texture, a wire texture does not necessarily imply large numbers of small angle boundaries between grains. In a wire texture there is a preferred family of planes lying perpendicular to the extrusion axis. This does not necessarily imply that there is a preferred orientation normal to the extrusion axis. The crystalline grains may be rotated about the extrusion axis and still have the wire texture as illustrated in fig. The result is the grain boundaries parallel to the extrusion direction are predominantly tilt boundaries, those perpendicular to the extrusion direction are twist boundaries and those in between have both tilt and twist components. Upon first glance this appears to be insufficient to promote bimodal grain growth, but the microstructure of this material does evolve in a bimodal fashion so a closer examination of the microstructure and texture characteristics is needed.

The bimodal grain growth in this material is characterized by a few grains growing quickly while the majority of the grains grow very slowly if at all. The grains which are growing in an abnormal manner are also elongated along the extrusion axis. This elongation could result from two possible scenarios. One, the grains which are growing in an abnormal manner only have the advantage in grain boundary migration in that direction. Or two, there is less resistance to grain boundary migration in general in that direction.

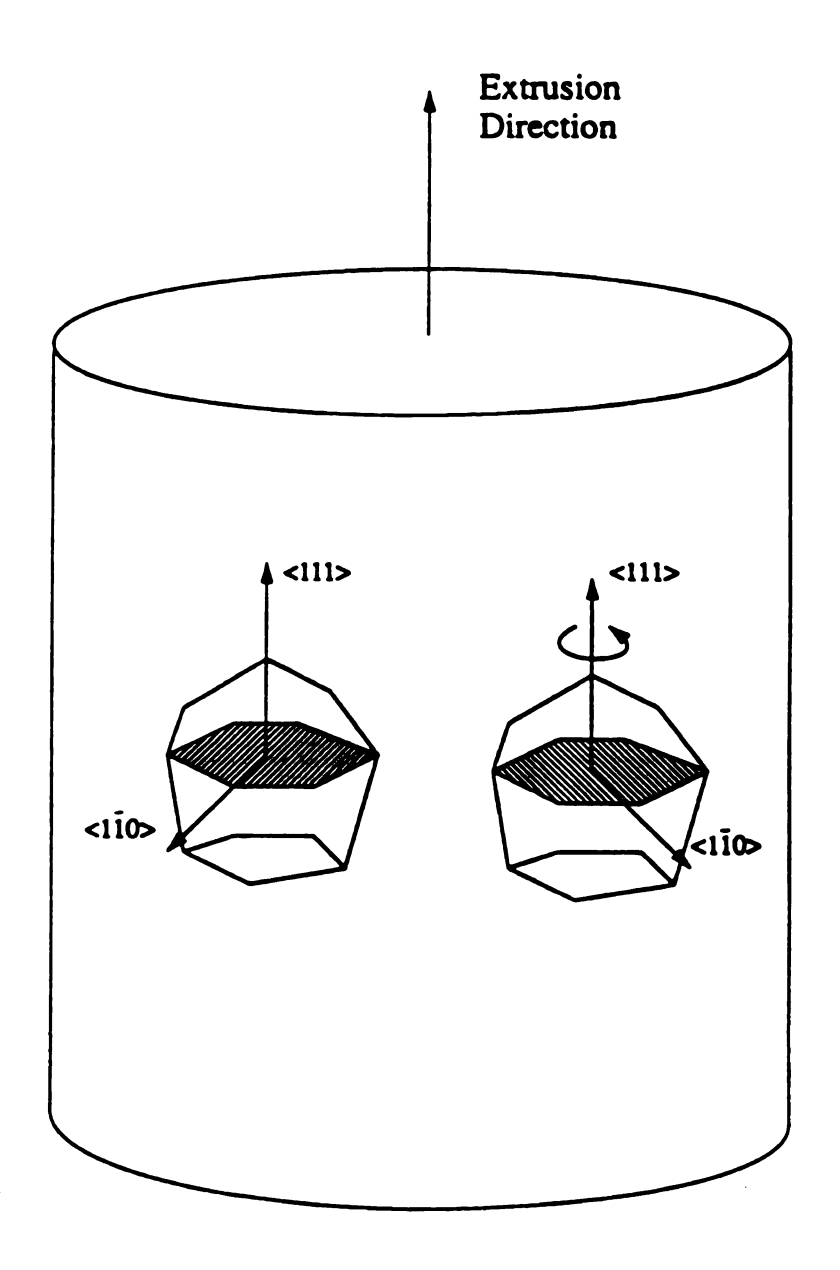


Figure 31. Illustration of rotational freedom in a material with a wire texture. After Hazzledine [74].

As discussed above, in a wire texture the twist boundaries generally run normal to the extrusion direction with tilt boundaries parallel. Examining the results of the EBSP analysis we can see that the orientations of the abnormal grains are random in the single extruded material without boron (fig. 21d) and grouped well away from the <111> direction for the materials with boron (figs. 22d and 23c). These results imply that it is, in fact, boundaries with tilt components normal to the extrusion direction that were free to migrate. This can be concluded since grains with pure twist boundaries normal to the extrusion axis would have the <111> orientation of the original matrix. Only grains with orientations away from the <111> wire texture will have tilt components normal to the extrusion axis. This supports the first theory if high angle tilt boundaries have higher migration rates than twist boundaries since the abnormal grains are the only grains to have high angle tilt boundaries normal to the extrusion axis. There is some evidence to support this argument as several studies have documented differences in migration rates for high angle twist and tilt boundaries [75,76].

Work by Yoshida el al. [76] strongly suggests <111>
tilt boundaries are more mobile then <111> twist boundaries.
Working with single crystals of aluminum, Yoshida et. al.
elongated then annealed the aluminum to examine the
recrystallization behavior. Most of the crystals were
extended 20% with others ranging from 10% to 50%. This

deformation range was used to avoid spontaneous recrystallization during the anneal. Before annealing, one end of the crystals were severely cold worked to provide nucleation sites. They found that while in the initial stages of recrystallization there was no preferred orientation and the number of <111> twist boundaries relative the initial matrix was consistent with the <111> tilt boundaries. This changes, however, by the end of recrystallization where grains with <111> twist boundaries were not present and grains with <111> tilt boundaries dominated the crystals. From this they concluded the tilt boundaries were more mobile then the twists.

The second scenario which could produce directional grain growth in this material would be if the barriers to grain boundary migration are stronger parallel to the extrusion direction than normal to it. This also seems likely when considering the shape and direction of the oxide stringers present in the material. It is evident in all of the micrographs that the stringers are very well aligned along the extrusion axis. In this configuration they act, in effect, very much like bars or rods of oxide running along the length of the material. This situation is very similar to that of a material containing oriented needle shaped inclusions. If we make the assumption this material behaves in a similar manner, we may compare the zener pinning forces for longitudinal and transverse grain boundary migration.

Calculations of zener pinning forces predict that needle shaped particles exert a much larger drag force on boundaries migrating transversely against the length of the particle then boundaries moving along the length of the particle [65]. In a material where needle shaped particles are well orientated this would result in much less resistance to migration in the direction along the particle length as opposed to normal to the particles. Ryum el al. [65] illustrated this point by calculating the drag forces on ellipsoidal particles. Figure 32 shows the two cases examined. Case one models migration along the length of the particles while case two models migration across the width. Working under the assumptions that the grain boundary energy is constant, the particle is incoherent with the matrix and the hole the particle makes in the grain boundary is planer, Ryum el al. came up with the following equations for the drag forces.

where,

case 1 
$$F_c = F_s (2e^{-1/3}/(1+e))$$
,  $F_c = drag$  force from ellipsoid shaped particle,  $F_s = drag$  force from spherical particle of 
$$equal \ volume,$$
 case 2  $F_c = (F_s/p)(1+2.14e)e^{-1/3}$   $e = b/a$ ,  $p = pie$ .

Figure 33 shows a plot of these equations for variations in eccentricity. From these calculations the authors concluded

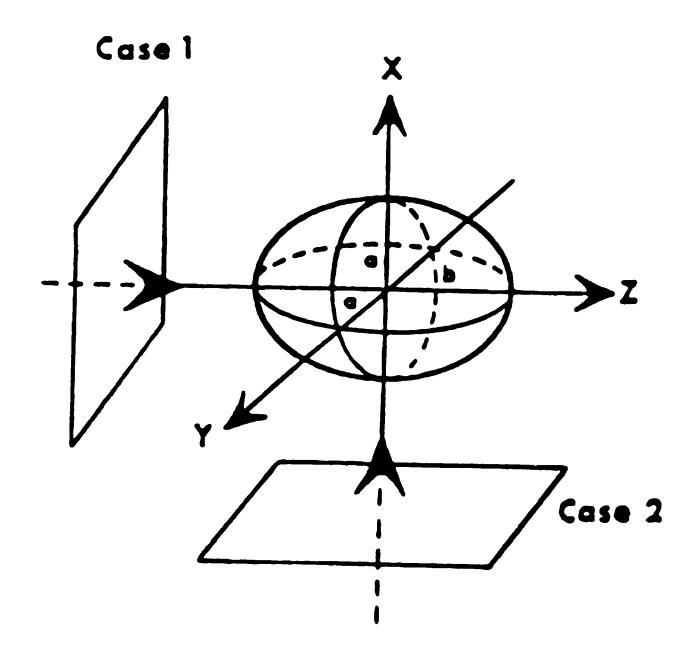


Figure 32. The two geometries of a grain boundary/particle interaction as discussed above [65].

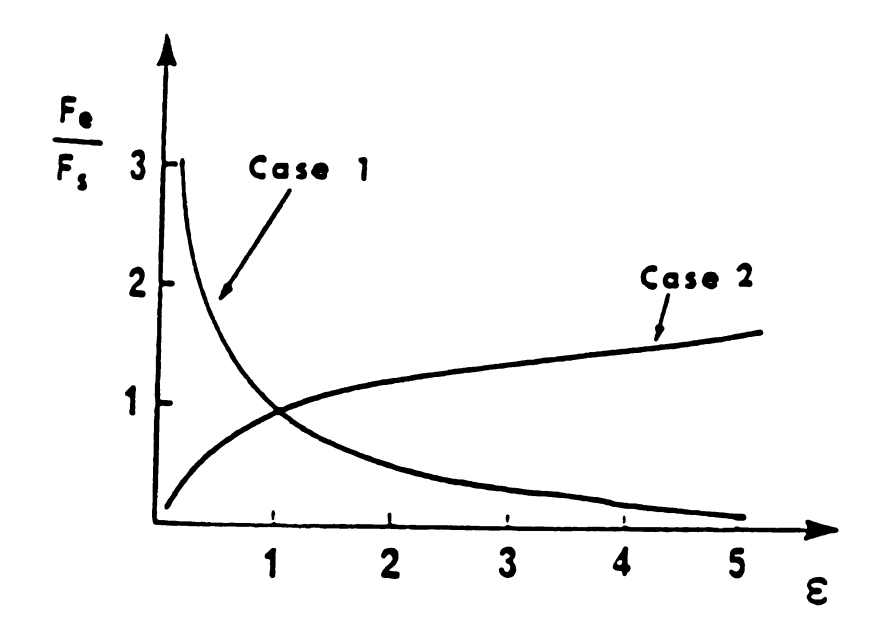


Figure 33. Plots of the relative drag forces produced by an ellipsoidal particle for variations in eccentricity for the two cases described above. The forces are normalized against the drag force of a spherical particle F. [65].

the drag force normal to the particle is from 2 to 4 times larger than the drag force parallel to the particles.

It is obvious that normal grain growth under these conditions would result in oblong shaped grains due to the directional nature of the resistance to grain boundary migration. The material in this study is an example of a material with well aligned particles but the normal grain growth rates at low temperatures are so slow no conclusion can be drawn. This effect is, however, apparent at higher temperatures where bimodal grain growth occurs. During the bimodal growth only a limited number of grains were free to migrate but these grains do show the oblong shape expected from growth under these conditions.

# A Theory on Bimodal Grain Growth in Wire Textured Materials

Based on the above argument that there is less drag in the longitudinal direction, a theory may be developed to explain the bimodal grain growth observed in this material. At the onset of grain growth, we may predict that during these early stages the initial growth would only be in the direction of least resistance because the activation energy necessary to overcome the particles would be reached in that direction before any other. This situation may result in a temperature range where grain boundaries normal to the extrusion axis will have sufficient energy to overcome the particles and migrate along the stringers while those parallel to the extrusion axis will not.

These conditions will change as grain growth proceeds because the pressure from grain boundary curvature in the transverse direction will increase. As a single grain, which is surrounded by stagnant grains, grows and elongates in the longitudinal direction, the grain boundary curvature in the transverse direction will increase, resulting in a increased the driving force for migration. The driving force will at some point becomes sufficient to overcome the drag forces and migration in the transverse direction can then proceed. The migration rates in the transverse direction will still be slower than in the longitudinal direction as the drag forces will be larger, so the oblong grain shape will persist during grain growth.

This theory may be taken a step further if we assume that we are operating in the temperature range described above. For the initial stage of grain growth only grain boundaries normal to the extrusion direction need be considered as those parallel to the extrusion direction are assumed to be pinned. This assumption results in a somewhat specialized texture. A large majority of the boundaries will be twist boundaries with only very small tilt components. As previously discussed, twist and low angle tilt boundaries have low mobility so any high angle tilt boundaries present in the matrix will migrate at a much higher rate than the surrounding boundaries. Figure 34 illustrates this point. This situation would result in abnormal grain growth by grains with high angle tilt

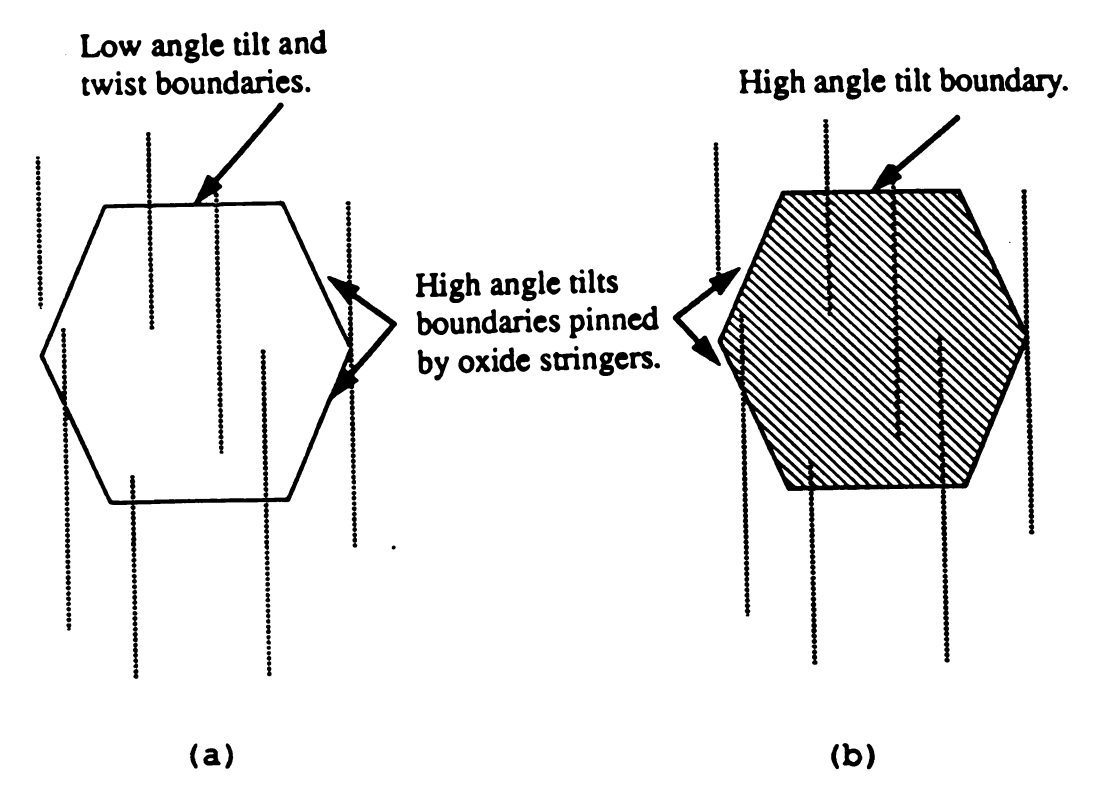


Figure 34. Illustrations representing the (a) a slow growing matrix grains and (b) a grain which may grow in an abnormal manner.

boundaries running normal to the extrusion axis. The materials in this study which grew in an abnormal manner possessed orientations tilted well away from the original wire texture, providing the high angle tilt boundaries. Additionally, they were also oblong in shape. This evidence support this theory but further investigation is required to substantiate this proposed mechanism for bimodal grain growth.

Further experimental evidence to support the theory that high angle grain boundaries have higher mobilities in the presence of particles was found by Tweed, et.al. [77,78]

who examined grain growth in an aluminum matrix containing alumina particles. Examining individual grain boundaries in non-textured aluminum they found that while all low angle boundaries were pinned by the alumina particles, only half of the high angle boundaries were pinned. Again, this suggests a difference in the activation energy required for low and high angle boundaries to overcome the pinning effect of particles.

#### Texture

A closer look at the EBSP results shows a large, well organized shift in orientations away from the <111> direction for the abnormal grains in the materials containing boron. In contrast, the material without boron does not display such a uniform shift in orientation. are no other differences in the materials or the processing. Therefore, it may be concluded that the boron is responsible for the difference in results. An explanation for this can be hypothesized here but further investigation is required to support any theory. The explanation for this is going to be linked to the grain boundaries and there ability to migrate. It is already known that boron additions in this material tend to segregate to grain boundaries [5]. increased boron concentration around the grain boundaries will cause drag as the boundaries try to migrate. There is evidence [18] that at certain angles, tilt boundaries set up in atomic configurations that are less susceptible to

impurity drag effects then other angles. This may be the situation in the boron containing materials. The material without boron would not have the drag forces produced by the boron so high angles boundaries in general may have enough mobility to over come the pinning forces and migrate. In the boron-rich materials however, only certain high angle boundaries are free to move.

The bimodal growth observed in the single extruded Fe-40at%Al with boron heat treated at 1100°C, and the double extruded Fe-40at%Al with boron heat treated at 1050°C are very similar. The growing grains all had orientations well away from the <111> wire texture of the matrix implying a large tilt component in the grain boundaries normal to the extrusion axis. If, as was suggested earlier, this material is viewed as a specialized textured these results correspond well with several of the theories and computer simulation on grain boundary migration [42,44].

In recent years computer simulations of grain growth have become very sophisticated [79-81] and, in turn, have made valuable contributions to our understanding of the grain growth process. Simulations of bimodal [43,81,82] grain growth have been performed to examine the kinetics and driving forces of bimodal growth in textured and non-textured material. Simulations by Rollett et.al.[43] of bimodal growth in textured materials produced microstructures similar to those observed in the powder processed materials examined in the current study. Several

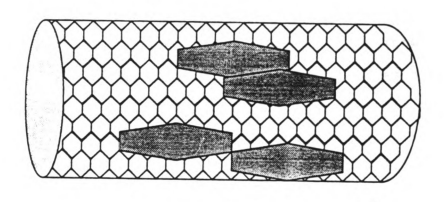
different approaches were used in these simulations with each giving slightly different results. The simulations which produced microstructures most like the ones observed in this study assumed variations in grain boundary mobility as the primary factor affecting grain growth.

Recent theoretical work [44,83] suggests that bimodal grain growth in textured materials is not abnormal at all, but what should be expected in textured materials where a few grains with high mobility are surrounded by a matrix of grains with low mobilities. Abbruzzese and Lucke [44] have shown that a few grains with high mobility boundaries in a textured matrix leads to bimodal grain growth. Furthermore, these authors argue that the concept of a critical radius, where all large grains grow preferentially over small grains, does not seem to apply to textured material, which eliminates the requirement that abnormal grain growth be initiated by unusually large grains.

# Macroscopic Behavior

In the results section it was noted that the bimodal grain growth was not uniform along the length of the extruded samples. Transverse sections with no evidence of abnormal grain growth were found only a few millimeters away from section displaying large areas of abnormal growth. Figure 35 shows a diagram illustrating the random nature in which the bimodal grain growth occurred. This situation could result from a number of causes such as inconsistencies

during extrusion or uneven heating, but the most likely explanation is simply the random nature in which bimodal grain growth occurs.





Original matrix grains from as extruded condition.



Abnormal grains.

Figure 35. Illustration of the random nature in which the bimodal grain growth in this material occurred.

### After 1200°C heat treatment

### Microstructure

The only sample heat treated above 1100°C was from the single extrusion material which was heated to 1200°C. The microstructure of this material shows normal grain growth during heat treatment. One possible explanations for this somewhat surprising result is that at 1200°C the activation energy required for the majority of the boundaries to overcome the pinning forces of the oxides may have now been reached. This would allow the matrix grains to grow much faster so the grains with orientations well away from the <111> wire texture would not have such a large growth advantage. With no great difference in the rates of grain growth, bimodal grain growth will not occur.

#### Texture

The texture of this material has become weaker and started to shift to the <221> and <110> directions. The new texture is a result of a dissipation of the original <111> texture by normal grain growth. This can be understood by starting with the inverse pole figure of the single extruded Fe-40at%Al with boron then imagine the effect a slow continuous shift to the <110> direction. The sharp <111> texture dissipates the fastest as grains with initial orientations tilted off the wire texture would have more large angle tilt grain boundaries then those on the wire texture. Another important feature to note is that at this

temperature the <111> oriented grains no longer appear to have an advantage during grain growth. At 1200°C the activation energy required to overcome the pinning effect of the particles has now been reached by all grain boundaries, so no one orientation is preferred during grain growth. This point will be discussed further in the final section of the discussion chapter.

## Cast Material

### Microstructure

The microstructure of the cast and extruded material differs from that of the powder processed material in two major ways. First, the grain size of the cast material is much larger. This is due mainly to the large grain size of the material prior to extrusion. Second, the cast material is much cleaner then the powder processed material. There are no oxidized surfaces of particles to produce the high density of oxide stringers seen in the powder processed material. This difference in material cleanliness plays an important role in the microstructural evolution of the material. As discussed earlier, it is the oxide stringer which are believed to be the catalyst for the bimodal grain growth seen in the powder processed material. Correspondingly, no bimodal grain growth was observed in this study in the cast and extruded material.

#### Texture

The cast Fe-40at%Al without boron displayed a <111> texture very similar to that seen in the powder processed material, indicating little change in the extrusion process between the cast and powder processed materials. behavior of the cast Fe-40at%Al material with boron is quite different from that of the powder processed material. contrast to the <111> texture of the powder processed material after extrusion, the cast material displays a <110> texture with a <111> component. The reason for this change in preferred orientation is not clear. It may be that the large initial grain size and boron addition resulted in incomplete recrystallization. Large grain sizes have been found to require higher temperatures before recrystallization will commence in cold worked material [47]. The boron additions will also acting to retard the nucleation processes by slowing subgrain growth. This would account for the <111> texture observed in the cast material without boron and the double <110>, <111> texture observed in the cast material with boron.

Upon heat treatment grain growth proceeds in a normal fashion with evidence of a subtle shift in preferred orientation from the <110> direction to the <211> direction. This same shift in preferred orientation has been observed in similar cast and extruded material after heat treatment at 1000°C by other researchers [1].

### Comments

In the 1200°C section it was argued that at this temperature the activations energy necessary to over come the pinning effects of the oxides was reached allowing for normal grain growth. Normal grain growth was also seen in the cast materials during heat treatment at all temperatures. Normal grain growth for this or any material should naturally dissipate a strong wire texture due to the theory that the grains with orientations away from the wire texture will have the most high angle grain boundaries and therefore high mobility boundaries. Evidence of this process is seen in the powder processed material heat treated at 1200°C and the cast materials. But when the powder processed material was heat treated at 1000°C what little grain growth there was acted to intensify the <111> texture. The fact that oriented growth is not seen in materials heat treated at temperatures high enough to overcome the oxide stringers or in the cast material which has no stringers suggests very strongly that the oriented growth is related to the oxide stringers.

In this material the oxide stringers play a vital role in triggering bimodal grain growth. It is conceivable, however, that a extremely tight single component wire texture would not require a pinning mechanism to trigger bimodal growth. In a extremely tight wire texture with no pinning mechanisms, grain growth along the extrusion axis would still be slow due to a lack of high angle tilt

boundaries. It is possible that a grain oriented well away from the texture could grow in a abnormal manner if its growth advantage along the extrusion axis is very large.

### CONCLUSIONS

- 1) Hot extrusion of the pre-alloyed FeAl powders produces a fine grained equiaxed microstructure. The oxide surfaces of the powders broke up during extrusion to produced oxide stringers in the material that run parallel to the extrusion axis. The oxide stringers run through the grains in a random nature indicating they did not restrict recrystallization during the extrusion process. There was very little grain growth during heat treatments at 1000°C due primarily to the network of oxide stringers pinning the grain boundaries.
- 2) Abnormal grain growth was been observed in the powder processed materials after heat treatments above 1000°C. The grains which grew in an abnormal fashion posessed orientations well away from the <111> wire texture. Having orientations well away from the <111> wire texture implies these grains had high angle grain boundaries normal to the extrusion axis. Additions of boron caused to limit the range of orientations which grew in an abnormal manner.
- 3) A theory was developed to explain the abnormal grain growth obseved in this material. It was proposed that the combination of the wire texture and oxide stringers acted to promote abnormal grains growth. Combining the two created a temperature range where high angle tilt boundaries normal to the extrusion axis have sufficient mobility to overcome the

|  |  | ! |
|--|--|---|
|  |  |   |
|  |  |   |
|  |  |   |
|  |  |   |
|  |  |   |
|  |  |   |
|  |  |   |
|  |  |   |
|  |  |   |
|  |  |   |

pinning oxides while the matrix grains do not.

- 4) Material that was produced by the extrusion of cast billets did not display abnormal grain growth. It is believed the lack of inclusions in this material resulted in normal grain growth because there were no particles to impied low mobility boundaries.
- 5) B2 FeAl produced by hot extrusion of a pre-alloyed powder develops a <111> wire texture when extruded between 800°C and 1077°C. The intensity of the <111> component of the texture increases between these two temperatures as does the grain size. It is believed that <111> oriented grains grow preferencially in this temperature range. Increases in the extrusion temperature then aid the preferred growth, resulting in a increase in the intensity of the <111> wire texture.

#### REFERENCES

- 1. B. Schnidt, P. Nagpal and I. Baker, Proceeding MRS 131 (1989) 755.
- 2. P.R. Munroe and I. Baker, J of Mat. Sci., 24 (1989) 4246.
- 3. M.A. Crimp, Phd Thesis, Case Western Reserve University, Cleveland, Ohio. 1987. Micrographs from unpublished work.
- 4. D.J. Gaydosh and M.V. Nathal, Scripta Met, 24 (1990) 1281.
- 5. C.T. Liu and E.P. George, Scripta Met, 24 (1990) 1285.
- 6. M.A. Crimp and K. Vedula, Mat. Sci. and Engin., 78 (1986) 193.
- 7. T. Yamagata and H. Yoshida, Mat. Sci. Engin., 12 (1973)
- 8. Y. Umakoshi and M Yamaguchi, Phil. Mag., A 41 (1980) 573.
- 9. I. Baker and D.J. Gaydosh, Mat. Sci. and Eng., 96 (1987) 147.
- 10. J.D. Whittenberger, Mat. Sci. and Eng., 57 (1983) 77.
- 11. J.D. Whittenberger, Private Communication.
- 12. P. Nagpal, and I. Baker, Private Communication.
- 13. S. Strothers, PhD. Dissertation, Case Western Reserve University.
- 14. D.J. Gaydosh, S.L. Draper, R.D. Noebe and M.V. Nathal, Mat. Sci. and Eng., In Press.
- 15. Kingery, Bowen, Uhlmann, <u>Introduction to Ceramics</u>.
  John Whiley & Sons, New York, 1976.
- 16. Reed-Hill, <u>Physical Metallurgy Principles 2nd Edition</u>. Brook/Cole Engineering Division, California, 1973.
- 17. Ralph, <u>The Structure and Energy of Grain Boundaries</u>. The Chameleon Press Limited, London, England. 1976.
- 18. Aust and Rutter, <u>Recovery and Recrystallization of Metals.</u>

- Gordon and Breach Publishers, New York, 1962. 131.
- 19. Gordon and Vandermeer, <u>Recrystallization</u>, <u>Grain Growth</u> and <u>Texture</u>. ASM, Metals Park, Ohio, 1966 205.
- 20. Grant, Porter, Ralph, J. of Mat. Sci., 19 (1984) 3554.
- 21. L.S. Shvindlerman and B.B. Straumal, Acta Metall., 33 (1985) 1735.
- 22. G. Herrmann, H. Gleiter and G. Baro, Acta Metall., 24 (1976) 353.
- 23. V. Randle and A. Brown, Phil. Mag., A59 (1989) 1075.
- 24. T. Takasugi and O. Izumi, Acta Metall., 31 (1983) 1187.
- 25. G.H. Bishop and B. Chalmers, Scripta Met., 2 (1968) 133.
- 26. B. Chalmers and H. Gleiter, Phil Mag, A23 (1971) 1541.
- 27. M.F. Ashby, F. Spaepen and S. Williams, Acta Metall., 26 (1978) 1647.
- 28. G.J. Wang, A.P. Sutton and V. Vitek, Acta Metall., 32 (1984) 1093.
- 29. K. Jagannadham and M.J. Marcinkowski, Phys. Stat. Sol.(a), 54 (1979) 715.
- 30. M.J. Marcinkowski and K. Jagannadham, Phys. Stat. Sol.(a), 50 (1978) 601.
- 31. Gleiter, Acta Metall., 17 (1969) 565, 853.
- 32. D.W. Bainbridge, C.H. Li and E.H. Edwards, Acta Metall., 2 (1954) 322.
- 33. C.H. Li, E.H. Edwards, J. Washburn and E.R, Parker, Acta Metall., 1 (1953) 223.
- 34. C.M.F. Rae and D.A. Smith, Phil. Mag., A41 (1980) 477.
- 35. Lucke, Rixen, Rosenbaum, <u>The Nature and Behavior of Grain Boundaries</u>. AIME, Plenum Press, New York, 1972. 245.
- 36. Shewmon, <u>Recrystallization</u>, <u>Grain Growth</u>, <u>and Texture</u>. ASM, Metals Park, Ohio, 1966. 165.
- 37. Gleiter, Material Science and Engineering, 52 (1982) 91.
- 38. Wang and Vitek, Acta Metall., 34 (1986) 951.

- 39. Rouag, Vigna, and Penelle, Acta Metall. 38 (1990) 1101.
- 40. C.H. Worner, S. Romero and P.M. Hazzledine, J. of Mat. Res., in press.
- 41. C.V. Thomson, H.J. Frost and F. Spaenen, Acta Metall. 35 (1987) 887.
- 42. D.J. Srolovitz, G.S. Grest and M.P. Anderson, Acta Metall., 33 (1985) 2233.
- 43. A.D. Rollett, D.J. Srolovitz and M.P. Anderson, Acta Metall., 37 (1989) 1227.
- 44. G. Abrruzzese and K. Lucke, Acta Metall., 34 (1986) 905.
- 45. R. Viswanathan and C.L. Bauer, Acta Metall., 21 (1973) 1099.
- 46. R.W. Cahn, <u>Physical Metallury</u>, <u>part 2, 3rd revision</u>, ed. by R.W. Cahn and P Haases, North-Holland Physics Publishing, New York.
- 47. R.D. Doherty, Metal Science, 8 (1974) 132.
- 48. S.S. Gorelik, <u>Recrystallization in Metals and Alloys</u>, Translated by V. Afanasyev MIR Publishers, Moscow. 1981.
- 49. J. Harase, R. Shimizu and T. Watanabe, Proc. 8th Int. Conf. on Textures and Materials (ICOTOM 8), ed. J.S. Kallend and G. Gottstein, TMS, 1988.
- 50. J. Harase and R. Shimizu, Acta Metall., 38 (1990) 1395.
- 51. W.G. Burgers and T.J. Tiedema, Acta Metall., 1 (1953) 234
- 52. P.A. Beck, Acta Metall., 1 (1953) 230.
- 53. P.S. Khadkikar, G.M. Michel and K. Vedula, Met. Trans., 21A (1990) 279.
- 54. I. Baker and D.J. Gaydosh, Metallography, 20 (1987) 347.
- 55. J.S. Kallend, U.F. Kocks, A.D. Rollett and H.R. Wenk, Mat. Sci. and Engin. A132 (1991) 1.
- 56. Venables and Harland, Phil Mag (27), 1193-1200, 1973.
- 57. M. Von Heimendahl, <u>Electron Microscopy of Materials</u>, <u>An Introduction</u>, Academic Press Inc. N.Y., N.Y.
- 58. J.S. Kallend, Kochs, Rollett and Wenk, Mat Sci and Eng,

- A132, 1991, 1.
- 59. D.J. Dingley, Scanning Electron Microscopy, 1981, 273.
- 60. D.J. Dingley, Scanning Electron Microscopy, 1984, 569.
- 61. P.M. Hazzledine, Czech. J. of Phys. B, 38 (1988) 431.
- 62. J.E. Burke, <u>Grain Control in Industrial Metallurgy</u>, ed. by J.E. Burke, R.L. Kenton, H. Burghoff and J.T. Hobbs, ASM, Cleveland, Ohio. 1949.
- 63. H. Burghoff, <u>Grain Control in Industrial Metallurgy</u>, ed. by J.E. Burke, R.L. Kenyon, H. Burghoff and J.T. Hobbs. ASM, Cleveland, Ohio. 1949.
- 64. J.E. Kenyon, <u>Grain Control in Industrial Metallurgy</u>, ed. by J.E. Burke, R.L. Kenyon, H. Burghoff and J.T. Hobbs, ASM, Cleveland, Ohio. 1949.
- 65. N. Ryum, O. Hunderi and E. Nes, Scripta Met., 17 (1983) 1281.
- 66. P.M. Hazzledine and R.D.J. Oldershaw, Phil. Mag. A, 61 (1990) 579.
- 67. J.D. L'Ecuyer and G. L'Esperance, Acta Metall., 37 (1989) 1023.
- 68. H. Fukutomi, S. Takagi, K. Aoki, M. Nobuki, H. Mecking and T. Kamoji, Scripta Met., 25 (1991) 1681.
- 69. W.B. Hutchinson, Met. Sci., 8 (1974) 185.
- 70. B.J. Duggan, M Sindel, G.D. Kohlhoff and K. Lucke, Acta Metall., 38 (1990) 103.
- 71. I.L. Dillmore and H. Katoh, Met. Sci., 8 (1974) 73.
- 72. T. Sheppard, N.C. Parson and M.A. Zaidi, Met. Sci., 17 (1973) 481.
- 73. T.R. Bieler, J.D. Whittenberger, R.D. Noebe, and M.J. Luton, Intermetallic Composites II, MRS Spring Meeting, San Francisco, in press.
- 74. P.M. Hazzledine, Personal communication, 1992.
- 75. S. Kohara, M.N. Parthasarathi and P.A. Beck. J. of Applied Physics, 29 (1958) 1125.
- 76. H. Yoshida, B. Liebmann and K. Lucke, Acta Metall., 7

(1959) 51.

- 77. C.J. Tweed, B. Ralph and N. Hansen, Acta Metall., 32 (1984) 1407.
- 78. C.J. Tweed, N. Hansen and B. Ralph, Met. Trans., 14A (1983) 2235.
- 79. M.P. Anderson, G.S. Grest and D.J. Srolovitz, Scripta Met., 19 (1985) 225.
- 80. G.S. Grest, M.P. Anderson, D.J. Srolovitz and A.D. Rollett, Scripta Met., 24 (1990) 661.
- B1. D.J. Srolovitz, M.P. Anderson, P.S. Sanhi and G.S. Grest, Acta Metall., 32 (1984) 793.
- 82. M.P. Anderson, D.J. Srolovitz, G.S. Grest and P.S. Sanhi, Acta Metall., 32 (1984) 783.
- 83. H. Eichelkraut, G. Abbruzzese, K. Lucke, Acta Metall., 36 (1988) 55.

# APPENDIX

The following is any information pertinent to the extrusion process, such as, extrusion temperature or reduction ratio. The extrusions were done at the NASA Lewis Research Center. The following information was taken from copies of the extrusion data sheets produced during extrusion.

Material: Fe-40at%Al

Temperature: 977°C

Reduction Ratio: 16:1

Pressure: 3100 psi

Hot Extrusion Data Sheet

Material: Fe-40at%Al-0.1B

Temperature: 977°C

Reduction Ratio: 16:1

Material: Fe-40at%Al

Temperature: 977°C

Reduction Ratio: 8:1

Pressure: 3100 psi

Hot Extrusion Data Sheet

Material: Fe-40at%Al

Temperature: 800°C

Reduction Ratio: 6:1

Material: Fe-40at%Al

Temperature: 1077°C

Reduction Ratio: 6:1

Pressure: 3100 psi

Hot Extrusion Data Sheet

Material: Fe-40at%Al-0.2B

Temperature: 977° €

Reduction Ratio: 8:1

Material: Fe-40at%Al-0.2B

Temperature: 1077°C

Reduction Ratio: 6:1

Pressure: 3100 psi

Hot Extrusion Data Sheet

Material: Fe-40at%Al-0.1B

Temperature: 977 ℃

Reduction Ratio: 16:1

Material: Fe-40at%Al

Temperature: 977°C

Reduction Ratio: 16:1

Pressure: 3100 psi

Hot Extrusion Data Sheet

Material: Fe-50at%Al

Temperature: 977° €

Reduction Ratio: 8:1

Material: Fe-50at%Al

Temperature: 800°C

Reduction Ratio: 6:1

Pressure: 3100 psi

Hot Extrusion Data Sheet

Material: Fe-50at%Al

Temperature: 1077°C

Reduction Ratio: 6:1

